Titre: Title:	Développement d'une diode supraluminescente à 1.3 µm
Auteur: Author:	Roy Saunders
Date:	1991
Type:	Mémoire ou thèse / Dissertation or Thesis
Référence: Citation:	Saunders, R. (1991). Développement d'une diode supraluminescente à 1.3 µm [Mémoire de maîtrise, Polytechnique Montréal]. PolyPublie. https://publications.polymtl.ca/57030/

UNIVERSITÉ DE MONTRÉAL

DÉVELOPPEMENT D'UNE DIODE SUPRALUMINESCENTE À 1.3 μm

par

Roy SAUNDERS

DÉPARTEMENT DE GÉNIE MÉCANIQUE

ÉCOLE POLYTECHNIQUE

RAPPORT DE PROJET PRÉSENTÉ EN VUE DE L'OBTENTION

DU GRADE DE MAÎTRE EN INGÉNIERIE (M.Ing.)

novembre 1991

To my family who have taken

my long hours of isolation

in their stride.

SOMMAIRE

Le présent rapport décrit en détail la première phase de la mise au point d'une diode supraluminescente (DSL) de 1,3 μm. Une DSL est un dispositif à semi-conducteurs qui émet de la lumière lorsqu'il est polarisé en sens direct. La puissance de sortie d'une DSL se rapproche de la puissance de sortie d'une diode laser à semi-conducteurs, mais la distribution spectrale de la puissance est similaire à celle d'une diode électroluminescente (DÉL). Grâce à ses propriétés, la DSL pourra être utilisée comme amplificateur optique, et dans les gyroscopes à fibre optique où un trés bon couplage aux fibres est nécessaire. Ce rapport fait état d'une spécification mise au point à partir d'une étude de marché des dispositifs qui sont nécessaires pour les amplificateurs optiques et les gyroscopes à fibres optiques. Ce projet vise à déterminer si un dispositif peut être fabriqué conformément à cette spécification à un coût acceptable.

Dans le cadre de ce projet, les plaquettes ont été dévelopées par épitaxie en phase vapeur aux installations de EG&G, à Vaudreuil, et par la technique "Metal-organic Chemical Vapor Deposition" (MOCVD) au Centre de recherches David Sarnoff, à Princeton. La zone active était constituée d'une couche quaternaire d'indium, de gallium, d'arsenic et de phosphore (InGaAsP), et la structure de la plaquette était basée sur celle de la DÉL courante de EG&G Optoelectronics, modifiée pour augmenter la densité du courant dans la région active. Les plaquettes ont été traitées avec des "ridge waveguides" pour assurer un certain guidage latéral et pour augmenter la puissance de sortie de la

zone active. Pour réduire les réflexions de lumière dans la zone active, deux précautions ont été prises: les barres ont été clivées à un angle de 85° par rapport aux guides et les facettes ont été recouvertes d'une couche antireflet d'oxyde de scandium. Pour obtenir le taux d'uniformité spectrale spécifié, le coefficient de réflexion devait être moins de 0,04%.

Les caractéristiques des dispositifs ont été établies et comparées à la spécification de base. Aucun des dispositifs n'a atteint la puissance de sortie nécessaire à la limite de courant de polarisation spécifiée et la variation spectrale de tous les dispositifs était inférieure à la spécification. Pour déterminer s'il était possible d'améliorer la DSL, un modèle de la puissance de sortie et de la variation spectrale par rapport au courant de polarisation a été mis au point. Ce modèle permet d'étudier certaines propriétés de la plaquette et de la puce finale à l'intérieur dans un domaine de limites connues.

On a conclu qu'il était impossible de fabriquer des dispositifs à couche active InGaAsP conformément à la spécification de base. Les résultats du modèle montrent que la puissance de sortie pourrait être augmentée si l'on utilisait une couche active plus épaisse et un coefficient de réflexion plus bas. Si la limite du courant de polarisation spécifiée à 150 mA pouvait être portée à 160 mA, il serait possible d'atteindre la limite de puissance de sortie en apportant des modifications à la croissance.

Une étude de coût, basée sur un boîtier ordinaire, a montré qu'un rendement des assemblages de 66% et un rendement des plaquettes de 50% produisaient un coût inférieur à 500$ par dispositif pour une production annuelle de 1000 dispositifs.

ABSTRACT

This report describes in detail the first phase of the development of a 1.3 μm Superluminescent Diode (SLD). The SLD is a semiconductor device which emits light when forward biassed. The light output power can approach the output power of a semiconductor Laser Diode (LD) but the spectral distribution of the power is similar to a Light Emitting Diode (LED). These properties make the SLD an attractive component for optical amplifiers and fiber optic gyroscopes where low modal noise, immunity to optical feedback and high coupling efficiency to fibers are necessary. A specification developed from a market survey of devices required for optical amplifiers and fiber optic gyroscopes is presented in this report. The objective of this project is to ascertain if a device can be manufactured to this specification at a reasonable cost.

For this project wafers were grown by Vapor Phase Epitaxy (VPE) at EG&G Optoelectronics, Vaudreuil and Metal-organic Chemical Vapor Deposition (MOCVD) at the David Sarnoff Research Center (DSRC), Princeton. The active region contains a quaternary compound of indium, gallium, arsenic and phosphorus (InGaAsP) and the wafer structure was based on the standard EG&G Optoelectronics LED structure with some modifications to increase the current density in the active region. The wafers were processed with ridge waveguides to provide some lateral guiding and to increase the output power from the active region. Two precautions were taken to reduce reflections back into the active region; the bars were cleaved at an angle of 85° to the ridges and

an antireflection coating of scandium oxide was applied to the facets. A reflection coefficient of 0.04% was the target required to achieve the modulation index of the specification.

The devices were characterized for comparison to the baseline specification. None of the devices made the required output power at the specified drive current limit and the devices that were tested for wavelength failed the specification for modulation depth. In order to determine if it was possible to improve the SLD, a model of output power and modulation depth against drive current was developed. The model enabled certain properties of the grown wafer and the final chip to be explored within documented limits.

It was concluded that it was not possible to manufacture devices with an InGaAsP active layer to the baseline specification. The results from the model show that the device performance could be improved by using a thicker active layer and a lower reflection coefficient. If the drive current limit in the baseline specification could be increased to 160 mA, instead of 150 mA, then the output power limit could be met with modifications to the wafer growth. The specified modulation depth could be met with modifications to the processing approach.

A costing exercise, based on the 14 pin dual-in-line package, showed that a 66% assembly yield and a 50% wafer yield would give a cost of less than $500 per device for a throughput of 1000 devices per annum.

RÉSUMÉ

Une étude de marché informelle a été utilisée pour formuler une spécification sur la diode supraluminescente (DSL):

a) La puissance optique de sortie minimale d'une fibre monomode est de 1 mW à 150 mA.

b) Le taux minimal de modulation spectrale est de 10%.

c) La longueur d'ondes est de 1300 nm +/- 20 nm.

d) La largeur spectrale minimale à la puissance médiane est 15 nm.

e) Le domaine de températures de fonctionnement est de 10°C à 40°C et le domaine de températures d'entreposage est de 0°C à 75°C.

f) Le taux de variation maximal de la longueur d'onde au maximum du spectre en fonction de la température est de 0,7 nm/°C.

g) L'exigence de fiabilité: moins de 50% de perte de puissance de sortie en 25 ans.

Le projet vise à déterminer si un dispositif peut être fabriqué conformément à cette spécification à un coût acceptable. Si d'autres travaux de développement se révélaient nécessaires, les champs d'étude devraient être redéfinis, mais il faut d'abord évaluer la technologie dont EG&G Optoelectronics dispose actuellement.

Le cycle de producton de la DSL commence par le processus de croissance du cristal. Pour ce projet, les plaquettes ont été obtenues par épitaxie en phase vapeur et à l'aide de la technique MOCVD. Six couches d'une épaisseur, d'un alliage et d'une concentration de dopage différents ont été déposées sur un substrat spécialement préparé. La zone active était constituée d'une couche quaternaire d'indium, de gallium, d'arsenic et de phosphore (InGaAsP) entourée de phosphore d'indium (InP) dopé (n et p). Ces couches adjacentes ont une largeur de bande interdite plus élevée et un indice de réfraction plus bas que la couche active. Cette différence dans la largeur de bande interdite permet de confiner les électrons et les trous dans la zone active où ils se recombinent pour produire de la lumière. La différence d'indice de réfraction confine le mode optique près de la couche active de manière à réduire les pertes internes.

La structure de la plaquette est basée sur une structure de DÉL standard modifiée pour réduire l'effet de diffusion du courant de manière à augmenter la densité du courant dans la région active. Une couche d'arrêt d'attaque chimique a été introduite dans la structure, et les plaquettes ont été spécialement traitées avec des "ridge waveguides" afin d'assurer un guidage latéral. La couche d'arrêt d'attaque chimique est lentement dissoute par de l'acide chlorhydrique à 80% pendant que la couche de phosphore d'indium située au-dessus est rapidement enlevée. Grâce à cette caractéristique, on peut contrôler la formation des rainures et en assurer l'uniformité.

Après le traitement des "ridge waveguides", divers métaux ont été déposés par évaporation sur les deux côtés de la plaquette à l'aide des techniques courantes de métallisation et d'alliage de EG&G Optoelectronics. Les plaquettes ont ensuite été clivées en barres. Généralement, dans le cas d'une diode laser, les barres sont clivées à 90° par rapport aux "ridge waveguides" de manière à créer une cavité de Fabry-Pérot. Cependant, puisque dans ce cas il fallait éviter que les facettes ne soient réfléchissantes, les barres ont été clivées à un angle de 85° par rapport aux rainures. Toute lumière sortant du dispositif est réfléchie dans les zones non pompées de la couche active. Cette précaution est nécessaire pour éviter la formation de modes longitudinaux qui pourraient faire varier la répartition spectrale de la puissance de sortie.

Une couche antireflet d'oxyde de scandium a été déposée par évaporation sur les facettes clivées à l'aide d'un évaporateur à faisceau éléctronique. L'oxyde de scandium est utilisé chez EG&G Optoelectronics dans la fabrication des puces DÉL afin d'éviter l'apparition de modes longitudinaux à basse température, et dans la fabrication du DSL afin d'éviter que la lumière ne soit réfléchie dans la zone active. Après l'application de la couche optique, les barres sont découpées en puces.

Les puces ont été ensuite soudées sur une electrode metallique au moyen de soudure d'étain/plomb, la zone active étant placée près de l'electrode metallique. La partie de l'electrode sur laquelle repose la puce est faite d'un alliage de cuivre et de tungstène choisi parce que son coefficient de dilatation correspond à celui du phosphore

d'indium. Cela évite que la puce ne puisse subir des contraintes pendant le soudage. Après le soudage, la puce a été nettoyée et l'autre contact a été fait au moyen d'un fil en or de 0,001 po.

Les caractéristiques du dispositif ont été établies, puis comparées à la spécification de base. La puissance de sortie a été mesurée en plaçant le dispositif directement devant un détecteur à grande surface et en augmentant le courant de polarisation. Aucun des dispositifs n'a atteint la puissance de sortie nécessaire, à la limite du courant de polarisation spécifiée, et certains dispositifs n'ont pas montré de caractéristques supraluminescentes. La distribution spectrale de la puissance de sortie a été mesurée sur deux dispositifs au moyen d'un interferomètre, et la variation spectrale calculée était inférieure à la limite spécifiée.

Pour déterminer s'il était possible de développer des plaquettes et de les traiter conformément à la spécification de base, un modèle simple donnait la puissance de sortie et la variation spectrale par rapport au courant de polarisation a été mis au point. Le modèle permet d'étudier certaines propriétés de la plaquette et de la puce finale en fonction de limites connues. Pour supporter le modèle, le champ proche de certains dispositifs a été mesuré, comparé aux valeurs calculées et jugé conforme. La densité de courant de seuil de chaque plaquette a été mesurée. Le rendement quantique interne a été calculé et comparé à celui de modèle. Les valeurs du rendement interne des dispositifs à puissance plus élevée étaient conformes. La comparaison des résultats expérimentaux

et des résultats numériques est présentée dans le rapport. Le modèle a permis de démontrer que l'épaisseur optimale de la couche active est de 0.22 μm et non de 0.13 μm. Il serait alors possible d'augmenter la puissance de sortie de 100% mais il sera nécessaire de déterminer si la cavité peut soutenir des modes d'ordre plus élevé.

On a conclu qu'il était impossible de fabriquer des dispositifs à couche active InGaAsP conformément à la spécification de base. Les résultats provenant du modèle sont présentés et donnent la puissance de sortie pouvant être obtenue si on apporte de légères modifications à la structure de la plaquette. Il est difficile d'obtenir la puissance spécifiée surtout en raison de la perte de rendement due à la recombinaison Auger, on s'attend à ce que les nouveaux matériaux basés sur les couches contraintes soient, à cet égard, plus performants. Il serait avisé d'étudier ces matériaux avant de poursuivre l'etude du composant realisé à partir de l'InGaAsP ordinaire.

Les meilleurs dispositifs avaient un coefficient de réflexion de 0,1%, ce qui ne permettait pas d'obtenir la variation spectrale spécifiée. Les résultats provenant du modèle sont présentés et indiquent que la variation spectrale est réalisable avec un coefficient de réflexion de 0,04%. Des valeurs inférieures ont été présentées dans la documentation mais ne sont probablement pas réalisables sur une ligne de production. On explique comment améliorer l'angle de clivage, ce qu'il serait intéressant d'étudier plus à fond.

Ce projet portait également sur l'étude des coûts de production. Le rapport présente une étude détaillée des coûts en supposant que la spécification de base se rapportant au niveau de la puissance de sortie et à la variation spectrale soit modifiée pour correspondre aux résultats obtenus avec le modèle. En ce qui a trait à l'étude des coûts, on a supposé que la puce DSL serait montée sur un boîter ordinaire dans lequel seraient incorporés un module à effet-Peltier et une thermistor. En supposant en rendement d'assemblage de 66% en un rendement des plaquettes de 50%, les meilleurs coûts réalisables sont de 484$ pour chaque dispositif, pour une production annuelle de 1000 dispositifs.

ACKNOWLEDGEMENTS

The author would like to express his appreciation to the staff of EG&G Optoelectronics for their invaluable assistance. In particular, A. Moore, S. Kurtz, R. Shuyen Lee and A. Devito contributed their time and vast experience to this project.

The staff of the laboratories at the David Sarnoff Center were very supportive. The author would like to extend his appreciation to R. Enstrom, G. Alphonse and J. Andrews for their growth and processing work.

The professors at École Polytechnique have a profound knowledge and lively interest in opto-electronics. The author is grateful for their teaching, guidance and encouragement.

CONTENTS

LIST OF FIGURES

LIST OF TABLES

LIST OF GRAPHS AND PHOTOGRAPHS

LIST OF SYMBOLS

A	Gain coefficient
As	Sellmeier coefficient
Ba	Radiative constant
Bb/Ba	Radiative ratio
$B(n)$	Spontaneous radiative coefficient
Bs	Sellmeier coefficient
C	Auger coefficient
Cs	Sellmeier coefficient
d	Layer thickness
da	Active layer thickness
df	Fiber core diameter
d_1	Thickness of layer 1
d_2	Thickness of layer 2
$d\parallel$	Emitting region length parallel to the active layer
$d\perp$	Emitting region thickness perpendicular to the active layer
D	Normalized thickness
E	Energy of a photon
g	Gain per cm.
go	Gain per cm. including the confinement factor
g_{th}	Gain per cm. at threshold

G	Gain of a Fabry-Perot amplifier
$Gmax$	Maximum gain of the amplifier
$Gmim$	Minimum gain of the amplifier
Gs	Single pass gain
Gsm	Mean single pass gain
Io	Lateral current flow
Is	Current passing through the ridge
Ja	Current density in the active region
J_{th}	Threshold current density
k	Boltzmanns constant
ko, ko'	Propagation constants
l	Cavity length
Lo	Width factor
m	integer
M	Modulation depth
n	Carrier density
no	Carrier density for transparency
P	Optical output power
Pf	Optical power in the fiber
$Pmax$	Maximum output power
$Pmin$	Minimum output power
Psp	Spontaneous output power

q	Charge of an electron
R	Resistivity
Ra	Auger recombination rate
Rad	Radiance of a source
Rb	Spontaneous recombination rate
Rc	Reflection coefficient
Rs	Sheet resistivity
$Rsld$	Radiance of the SLD
R_1, R_2	Resistivities of layers 1 and 2
r_1, r_2	Field reflectivities of facets 1 and 2
Sy	Spreading width to one side of the ridge
t	Refractive index
t_1, t_2	Refractive indices of the cladding and active layers
T	Absolute temperature
w	Ridge width
x	Gallium composition
y	Arsenic composition
Z	Gain factor
α	Optical loss per cm.
αo	Optical loss per cm. including the confinement factor
Γ	Confinement factor
ηi	Internal quantum efficiency

ηo	Optical efficiency
$\Theta \perp$	Far field angle perpendicular to the plane of the active layer
$\Theta \parallel$	Far field angle parallel to the plane of the active layer
λ	Wavelength
λcen	Center wavelength
μ	Carrier mobility

LIST OF APPENDICES

INTRODUCTION

The Superluminescent Diode is not a new device, EG&G Optoelectronics and other manufacturers have made SLDs at 0.83 μm over the last few years. These devices contain an active region of a ternary compound of aluminium, gallium and arsenic (AlGaAs). Unfortunately there is a failure mechanism associated with this material. Dislocations in the crystal structure grow in the presence of recombining holes and electrons causing non-radiative recombination in the active region until, eventually, the device stops emitting light. Attempts to prevent dislocations starting by using better substrates and more careful processing have only been partially successful and available devices do not satisfy the requirements of the fiber optic gyroscope or the optical amplifier manufacturer.

Laser diodes, used in telecommunication applications at 1.3 μm, contain an active region of a quaternary compound of indium, gallium, arsenic and phosphorus (InGaAsP). The reliability of these devices has been demonstrated over many years and they do not degrade as quickly as the AlGaAs devices. The objective of this project is to ascertain if a SLD made with an InGaAsP active region can meet the other requirements of the fiber optic gyroscope and the optical amplifier manufacturer.

This development pushes two key technologies to the limit. The growth technology has to provide wafers with high gain and the wafer processing technology has

to reduce to a minimum the reflections from the end facets back into the Fabry-Perot cavity. There are a number of variables involved in both these technologies and it was unlikely that the first attempt would produce an optimum device, so a simple model of the key parameters was developed to determine what improvements would be required for the device to meet the baseline specification.

Apart from the technical considerations the finished device must cost less than $500 in production quantities. A device in a 14 pin dual-in-line package was configured on EG&G Optoelectronics materials requirement planning (MRP) system so that the cost could be estimated. The materials selected for the device were similar to a LED currently being manufactured at EG&G Optoelectronics and, wherever possible, conventional processes were utilized because their costs were known. A detailed cost simulation was carried out with the yields at each stage of manufacture included.

There are other technologies that can provide suitable sources for both optical amplifiers and fiber optic gyroscopes, for example the erbium doped fiber laser or other pumped crystals. These technologies are currently receiving a great deal of attention but may prove to be more expensive because they require more components.

SECTION 1

THE SPECIFICATION OF THE SUPERLUMINESCENT DIODE

1.1 GENERAL

The test conditions are a continuous wave (CW) current drive of 150 mA in a 23°C ambient. Some tests require different conditions and this is specifically stated in the text. The drive current of 150 mA is considered to be the maximum for this device, higher drive conditions could create heat dissipation problems in the fiber optic gyroscope or optical amplifier system. The device outline is a 14 pin dual-in-line package with a fiber pigtail, a thermoelectric cooler and thermistor are required to provide temperature control for the chip.

1.2 OPTICAL POWER

The fiber is a polarization maintaining, single mode type optimized for use at 1.3 μm. One preference is the AT&T rectangular fiber which has a core diameter of 8.5 μm and a numerical aperture about 0.1. The minimum optical power requirement is 1 mW from the fiber.

1.3 CENTER WAVELENGTH

The center wavelength, λcen, as measured at the center of the half power points of the spectral distribution plot of output power, is 1300 nm +/- 20 nm. This is illustrated in figure 1.

1.4 SPECTRAL MODULATION DEPTH

The spectral modulation depth is defined as the difference between Pmax and Pmin of the spectral envelope divided by the sum of Pmax and Pmin. For clarity, Pmax and Pmin are illustrated in figure 1. The spectral envelope has to be smooth for the spectral modulation depth to meet the maximum limit of 10%.

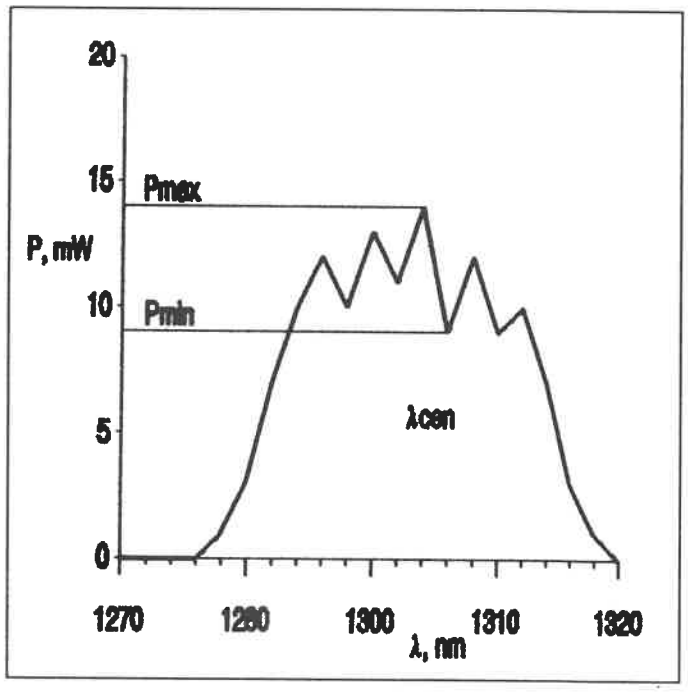

Figure 1 A schematic of the spectral distribution of output power

1.5 SPECTRAL WIDTH

The spectral width, as measured between the half power points of the spectral distribution plot of the output power, must be greater than 15 nm.

1.6 TEMPERATURE RANGE

The operating temperature range is 10°C to 40°C and a thermo-electric cooler is required to maintain a constant chip temperature. In this case, a thermistor is required to monitor the chip temperature and control the current driving the cooler. The storage temperature range is 0°C to 75°C.

1.7 CHANGE OF CENTER WAVELENGTH WITH TEMPERATURE

The maximum rate of change of peak wavelength with temperature over the operating temperature range is 0.7 nm/°C.

1.8 RELIABILITY

After 25 years in a constant ambient of 40°C +/- 3°C the optical output power must not drop by more than 50% of the starting power.

SECTION 2

THEORY

2.1 OUTLINE OF THE THEORETICAL APPROACH

The objective of the theory is to provide equations that show the relationship between the facet output power and drive current and between the modulation depth and drive current. The variables are known from the literature or are able to be measured.

The first part of the theory calculates the current flowing through the device for a given value of carrier density in the emitting region. The current path can be followed by referring to figure 2. The current flows through the metal contact into the ridge then through various layers and out through a metal contact on the substrate. The layers to the sides of the ridge are insulators but underneath the ridge the layers are doped and lateral spreading of the current occurs. This has to be taken into account when relating the current density in the active layer to the current flowing through the ridge. The current density in the emitting region is

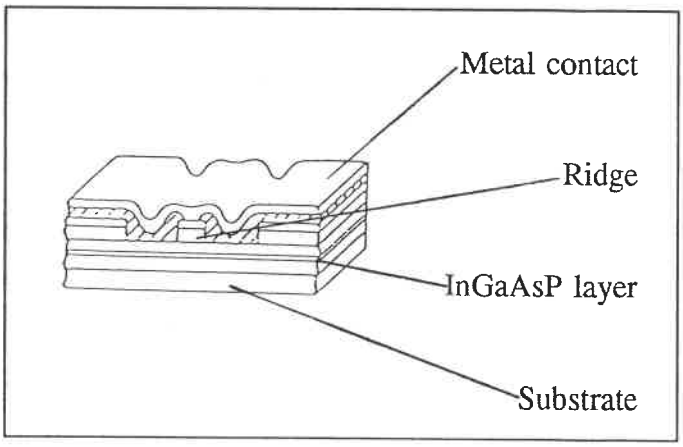

Figure 2 A schematic of the chip

related to the carrier density by various recombination mechanisms, both radiative and nonradiative.

It is possible, at this stage, to check the equations against measurements. The light emission from the SLD takes place from the active layer under the ridge and, with the aid of a microscope and video analyser, it is possible to measure the emitting length and verify the current spreading calculation. Another check can be made on the ratio of the radiative and nonradiative recombination rates. When the grown wafers are first characterized a piece of the wafer is removed, metallized and tested for threshold current. Later in the theory the relationship between internal quantum efficiency and threshold current density is shown. This value of internal quantum efficiency can be compared directly to the internal quantum efficiency calculated from the radiative and nonradiative recombination rates.

The SLD works by a spontaneously generated photon travelling along the active region and by its presence, stimulating the generation of other photons. The next part of the theory calculates the gain in the active region because of this process. For this the refractive indices of the active region and the cladding layers are calculated so that the confinement factor may be determined. The confinement factor is the proportion of the optical wave in the active region.

Once the optical efficiency is defined to take into account the random nature of the spontaneous emissions then the spontaneous output power can be calculated from the spontaneous recombination rate and the chip geometry. The output power from a facet can now be calculated from the spontaneous output power and the gain.

The spectral modulation depth is calculated as a ratio of the minimum and maximum gains of a Fabry-Perot amplifier. These gains are calculated directly from the total gain of the active region as previously determined.

The final part of the theory calculates the maximum coupling efficiency between the chip and the fiber in order to decide what value of facet output power is required to launch 1 mW into the fiber.

2.2 THE DRIVE CURRENT

2.2.1 The spontaneous radiative coefficient

When the device is forward biassed, photons are spontaneously generated in the active region. In terms of semiconductor physics, an electron in the conduction band recombines with a hole in the valence band to produce a photon. This describes a radiative recombination process but not all the carriers recombine in this way and an important nonradiative recombination process is described later in the theory.

The spontaneous recombination rate, Rb, is given by[1]

$$Rb = B(n)\ n^2 \qquad \text{cm}^{-3}\ \text{s}^{-1} \tag{1}$$

Where $B(n)$ is the spontaneous radiative coefficient, in $\text{cm}^3\ \text{s}^{-1}$, and n is the carrier density in carriers cm^{-3}. The spontaneous radiative coefficient is not independent of the carrier density and can be approximated by[1]

$$B(n) = Ba - Bb\ n \qquad \text{cm}^3\ \text{s}^{-1} \tag{2}$$

where Ba is the radiative constant that lies within the range 5×10^{-11} to 7×10^{-10} $\text{cm}^3\ \text{s}^{-1}$ and $Bb\ /\ Ba$ is the radiative ratio that lies within the range 1.7×10^{-19} to 2.2×10^{-19} cm^3. These values are documented by Agrawal and Dutta[1].

2.2.2 The Auger coefficient

In the case of the InGaAsP material, Auger recombination is the predominant nonradiative recombination mechanism. There are three major types of Auger recombination; a) band to band processes b) phonon assisted processes and c) trap assisted processes. In this case, the nonradiative recombination due to trap or surface recombination is ignored because the material is of a high quality.

The Auger recombination rate, Ra, is given by[1]

$$Ra = C\, n^3 \qquad \text{cm}^{-3}\ \text{s}^{-1} \tag{3}$$

where C is the Auger coefficient which typically lies within the range 3×10^{-29} to 9×10^{-29} $\text{cm}^6\ \text{s}^{-1}$. These values are again from Agrawal and Dutta[1].

2.2.3 The current density in the active region

The current density, Ja, at the active region can be calculated from the recombination rates[1]

$$Ja = q\, da\, (\, B(n)\, n^2 + C\, n^3\,) \qquad \text{A cm}^{-2} \tag{4}$$

where q is the electron charge in coulombs and da is the thickness of the active region in cm.

2.2.4 The composite sheet resistivity

In all the structures considered, there are several layers in which the current can spread. The current in the ridge is assumed to be evenly spread because of the high doping concentration in the capping layer. In the layers below the ridge, the amount of spreading is dependent on the resistivity, R, and thickness, d, of the individual layers.

The resistivity of a layer can be calculated from the equation

$$R = \frac{1}{n\ q\ \mu} \quad \text{ohm cm} \tag{5}$$

where μ is the mobility of the carriers in $cm^2\ V^{-1}\ s^{-1}$. The actual values of μ for the individual layers were extrapolated from Pearsall [10]. The composite sheet resistivity, *Rs*, can be calculated from the resistivities and thicknesses of the individual layers.

$$\frac{1}{Rs} = \frac{d_1}{R_1} + \frac{d_2}{R_2} + \ldots \quad \text{ohms}^{-1} \tag{6}$$

2.2.5 The lateral current flow

The lateral current flow in one direction only, *Io*, is given by[3]

$$Io = \left(\frac{0.104\ Ja\ l^2}{Rs} \right)^{\frac{1}{2}} \quad \text{A} \tag{7}$$

where *l* is the cavity length in cm. The factor 0.104 in this equation comes from doubling the exponential junction parameter mkT/q, where k is the Boltzmann constant, T is the absolute temperature and m is an integer. In this case, m is taken to be 2, in line with

semiconductor diode practice.

2.2.6 The current in the ridge

The current passing through the ridge, *Is*, is given by[3]

$$Is = \frac{0.104\ l}{Rs\ w}\left[\left[\frac{Io\ w\ Rs}{0.104\ l} + 1\right]^2 - 1\right] \quad \text{A} \tag{8}$$

where w is the ridge width in cm.

2.3 THE SUPPORT EQUATIONS

2.3.1 The spreading width

The spreading width is arbitrarily defined as the distance from the side of the ridge to a point where the current density falls to half the current density of the center of the active region. This definition, and the lateral current flow determined from equation (7), can be used to calculate the spread on one side of the ridge, *Sy* cm. The emitting width of the active region can be measured with a CCD camera and video analyser and the result compared to the total active width.

The spread is given by[3]

$$Sy = Lo \left[\left[\frac{Ja\ Lo\ l}{2\ Io} \right]^{\frac{1}{2}} - 1 \right] + \frac{w}{2} \quad \text{cm} \tag{9}$$

in equation (9) the width factor, Lo, is given by

$$Lo = \frac{0.104\ l}{Rs\ Io} \quad \text{cm} \tag{10}$$

The total active width is the ridge width plus twice Sy.

2.3.2 The internal quantum efficiency

The internal quantum efficiency, ηi, is defined as the efficiency at which electrons in the conduction band are able to generate a photon. For good quality InGaAsP layers, the contribution of nonradiative trap and surface recombination can be ignored. If the current density is below the threshold current density then ηi can be considered to be a simple ratio of the radiative and nonradiative recombination rates[1]

$$\eta i = \frac{Rb}{Rb + Rc} = \frac{B(n)\ n^2}{B(n)\ n^2 + C\ n^3} \tag{11}$$

When wafers are processed a small part is removed and the threshold current level is measured. From this measurement it is possible to determine the internal quantum efficiency, the equations for this are presented later in the theory.

2.4 THE OPTICAL OUTPUT POWER

2.4.1 The optical gain equation

The gain per cm, g, in the active region is given by[1]

$$g = A\ (\ n - no\ ) \qquad \text{cm}^{-1} \tag{12}$$

where A cm^2 is the gain coefficient, typically in the range 1.2×10^{-16} to 2.5×10^{-16} cm^2, n cm^{-3} is the injected carrier density and no cm^{-3} is the injected carrier density to achieve transparency or zero gain. Typical values for the transparency density lie within the range 0.9×10^{18} to 1.5×10^{18} cm^{-3}. These values are documented by Agrawal and Dutta[1].

2.4.2 The refractive index profile

The structures used to manufacture 1.3 μm LEDs and 1.3 μm pulsed LDs are similar, the main differences between these devices are the way the facets are prepared and the angle of the ridge to the facet. Both devices contain a quaternary layer of InGaAsP between layers of highly doped indium phosphide (InP). The refractive indices

of the quaternary and InP layers are calculated from a modified Sellmeier formula[5]

$$t^2 = As + \frac{Bs\ \lambda^2}{\lambda^2 - Cs} \tag{13}$$

where t is the refractive index and As, Bs and Cs are the Sellmeier coefficients and λ is the wavelength in μm. The coefficients need to be calculated for the quaternary layer,

$$As = 7.255 + 1.15\ y + 0.489\ y^2 \tag{14}$$

$$Bs = 2.316 + 0.604\ y - 0.493\ y^2 \tag{15}$$

$$Cs = 0.3922 + 0.396\ y + 0.158\ y^2 \tag{16}$$

where y is the arsenic composition of the quaternary given by

$$y = \frac{2.202\ x}{1 + 0.0659\ x} \tag{17}$$

and x is the gallium composition. The relationship between x and y is restricted by the requirement for the InP to be lattice matched to the quaternary. At 1.3 μm the quaternary layer contains 27% gallium so $y = 0.584$, $As = 8.09$, $Bs = 2.50$ and $Cs = 0.677$ which gives t as 3.50. In the case of InP, $y = 0$, so the calculations are easier, $As = 7.255$, $Bs = 2.316$ and $Cs = 0.3922$ which gives t as 3.20.

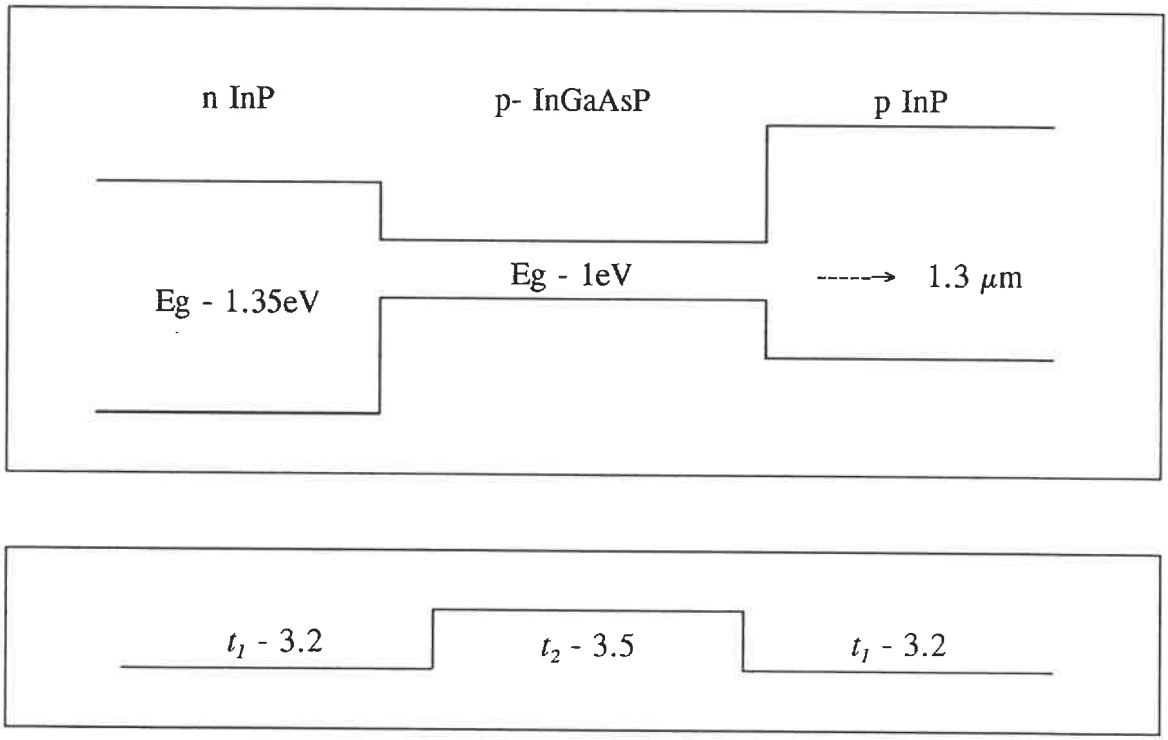

Figure 3 The idealized energy and band diagram and refractive index profile

2.4.3 The confinement factor

The confinement factor[2], Γ, is determined by calculating a normalized thickness D,

$$D = \frac{2\ \pi\ da}{\lambda} \left(t_1^2 - t_2^2 \right)^{\frac{1}{2}} \qquad \textbf{(18)}$$

where t_1 is the refractive index of the InP cladding layers, and t_2 is the refractive index of the InGaAsP active region.

It has been reported[2] that Γ is well approximated, to within 1% for $D < 2$, by

$$\Gamma = \frac{D^2}{2 + D^2} \qquad \textbf{(19)}$$

in which case, $\Gamma = 0.484$ for $da = 0.2\ \mu$m.

The confinement factor is the proportion of the optical wave which is contained in the active region of the device. The proportion of the optical wave in the adjacent layers is lost because it does not stimulate emission.

2.4.4 The single pass gain equation

Consider a semiconductor structure with a cavity consisting of an active region surrounded by uniformly doped layers, as idealized in figure 3, and with end facets which have negligible reflection. Then the gain of an optical signal, *Gs*, passing once through this structure, when there is no reflected signal at all, is given by [11]

$$Gs = \exp (\Gamma (g - \alpha) l) \qquad (20)$$

where α is the optical loss per cm from the processes not directly associated with the gain mechanism.

The spontaneous emission is not directional and will occur anywhere along the length of the cavity. As a photon passes through the active region other photons are generated as holes and electrons are stimulated to combine. The newly generated photons have the same wavelength and the same direction as the original photon. In the SLD chip every attempt is made to reduce facet reflections to ensure that each photon only passes once through the cavity. A photon generated at one end of the cavity will cause stimulated emission along the entire length of the cavity but a photon generated at the other end will cause little stimulated emission. If it is assumed that spontaneous emission occurs uniformly along the cavity then the average, single pass gain will be *Gsm*.

If equation (20) is written as

$$Gs = \exp (Z x) \tag{21}$$

where x cm is the distance along the cavity, then

$$Gsm = \frac{1}{l} \int_0^l \exp (Z x) dx \tag{22}$$

which becomes

$$Gsm = \frac{1}{l Z} \left(\exp (Z l) - 1 \right) \tag{23}$$

2.4.5 The optical efficiency

The calculation of the spontaneous power from a particular structure is made difficult by geometry and, unlike stimulated emission, spontaneous emission can result in a photon going in any direction. The optical efficiency, ηo, is defined, therefore, as the probability of a spontaneously generated photon exiting one facet of the chip. In LEDs the value of the optical efficiency will be low of the order of one percent.

2.4.6 The spontaneous output power

The energy of a photon, E, is given by

$$E = \frac{2.02\times10^{-19}}{\lambda} \quad \text{joules} \tag{24}$$

and the spontaneous emission rate is given by equation (1). The spontaneous output power, *Psp*, may be written as

$$Psp = \frac{2.02\times10^{-19}\ Rb\ \eta o\ l\ w\ da}{\lambda} \quad \text{W} \tag{25}$$

2.4.7 The output power

The output power, *P*, can be calculated from the spontaneous output power and the mean single pass gain by

$$P = Psp + Psp\ Gsm \quad \text{W} \tag{26}$$

2.5 THE SPECTRAL MODULATION DEPTH

2.5.1 The gain of a Fabry-Perot amplifier

The gain, G, of a Fabry-Perot amplifier is given by Henry[6] as

$$G = \frac{(1 - r_1^2) (1 - r_2^2) \exp [(go - \alpha o) l]}{[1 - r_1 r_2 \exp (2 i ko l)]^2} \qquad (27)$$

where r_1 and r_2 are the field reflectivities of both facets of the Fabry-Perot cavity and go and αo are the gain and optical losses including the confinement factor.

$$ko = ko' - i \frac{(go - \alpha o)}{2} \qquad (28)$$

where ko' is the propagation constant and

$$Rc = r_1^{\frac{1}{2}} = r_2^{\frac{1}{2}} \qquad (29)$$

where Rc is the reflection coefficient at the facets, assuming each facet is cleaved and coated similarly.

Equation (27) may be rewritten as

$$G = \frac{(1 - Rc^2)\, Gs}{1 + Rc^2\, Gs^2 - 2\, Rc\, Gs \cos(2\, i\, ko'\, l)} \qquad (30)$$

and, if Rc is not zero, then G undergoes a maximum and a minimum for values of $2iko'l$ equal to even and odd numbers of π.

$$Gmax = \frac{(1 - Rc^2)\, Gs}{1 + Rc^2\, Gs^2 - 2\, Rc\, Gs} \qquad (31)$$

$$Gmin = \frac{(1 - Rc^2)\, Gs}{1 + Rc^2\, Gs^2 + 2\, Rc\, Gs} \qquad (32)$$

2.5.2 The spectral modulation depth

The modulation depth, M, can now be calculated by

$$M = \frac{Gmax - Gmin}{Gmax + Gmin} \qquad (33)$$

and can be compared directly to measurements taken from a plot of the spectral distribution of the output power as described in section 1.

2.6 THE INTERNAL QUANTUM EFFICIENCY

If the power reflection coefficients at the two end facets are equal then the gain per cm at threshold, g_{th}, is[11]

$$g_{th} = \frac{1}{\Gamma}\left[\alpha + \frac{1}{l}\ln\left[\frac{l}{Rc}\right]\right] \quad \text{cm}^{-1} \tag{34}$$

The gain in an active region of InGaAsP quaternary which contains 28% gallium and 60% arsenic is given by[4]

$$g = 0.074\left[\frac{Ja\ \eta i}{da} - 3025\right] \quad \text{cm}^{-1} \tag{35}$$

and this equation can be used directly with equation (34) to give the internal quantum efficiency of the wafer when the threshold current density, *Jth*, is known.

$$\eta i = \frac{da}{Jth}\left[\frac{1}{0.074\ \Gamma}\left[\alpha + \frac{1}{l}\ln\left[\frac{1}{R}\right]\right] + 3025\right] \qquad (36)$$

and the result from this equation can be compared to the result of equation (11).

2.7 THE COUPLING EFFICIENCY

2.7.1 The optimum coupling efficiency between chip and fiber

If the radiance of a source, *Rad*, is defined as

$$Rad = \frac{P}{d\perp\ \Theta\perp\ d\parallel\ \Theta\parallel} \qquad \text{mW } \mu\text{m}^{-2}\ \text{sr}^{-1} \qquad (37)$$

where $d\perp$ is the emitting width perpendicular to the plane of the active region, in μm, and $d\parallel$ is the emitting length parallel to the plane of the active region, in μm. $\Theta\perp$ and $\Theta\parallel$ are the $1/e^2$ angles of the far fields, in radians. The far field is the distribution of the output power at a distance from the source and is used to measure the angular divergence of the emitted beam.

The maximum power that can be coupled into a fiber is obtained by equating the fiber radiance and the source radiance. For a diffraction limited gaussian beam, such as

a fiber,

$$\Theta\perp = \Theta\parallel = 1.27\ \frac{\lambda}{df} \qquad \text{rad} \tag{38}$$

where $df = d\parallel = d\perp$ and is the core diameter in μm. At a wavelength of 1.3 μm, for a fiber with a radiance *Rf*, equation (37) becomes

$$Rf = \frac{Pf}{(\ 1.27\ \lambda\ )^2} = 0.37\ Pf \qquad \text{mW}\ \mu\text{m}^{-2}\ \text{sr}^{-1} \tag{39}$$

where *Pf* is the power in the fiber.

The SLD is diffraction limited in the direction perpendicular to the active region, so equation (37) becomes

$$Rsld = \frac{P}{1.27\ \lambda\ d\parallel\ \Theta\parallel} \qquad \text{mW}\ \mu\text{m}^{-2}\ \text{sr}^{-1} \tag{40}$$

where *Rsld* is the radiance of the SLD.

The coupling efficiency is given by equating equation (39) and equation (40)

$$\frac{Pf}{P} = \frac{1.637}{d \| \Theta \|} \tag{41}$$

The emitting width of the SLD is 9 μm, typically, and the far field, parallel to the active region, is about 65°. This yields an optimum coupling efficiency of 16%. It would be prudent to assume that this efficiency is unobtainable on a production basis and that 10 mW from the facet of the chip would be required to achieve 1 mW in the fiber.

SECTION 3

EXPERIMENTAL APPROACH

3.1 DEVICES FROM WAFERS GROWN BY VAPOR PHASE EPITAXY

3.1.1 Vapor phase epitaxial growth

EG&G Optoelectronics used to grow wafers for pulsed LD and LED fabrication in a custom built vapour phase epitaxial (VPE) growth reactor. VPE is a crystal growth process whereby gases are used to deposit a solid semiconductor compound or alloy onto a substrate. In this process, the solid alloy composition is determined by the gas composition which can be linearly controlled by mass flow controllers. The gas is fed into the reactor over sources which are heated to 850°C. After mixing the vapor is transported to the substrate held in the deposition zone at 700°C. In order to grow multi-layer structures a "double barrel" reactor is used. In this case, different gases can be run through each tube and the substrate can be mechanically transferred from one tube to another in order to achieve a "clean" interface between the grown layers. The reactor was originally developed at the David Sarnoff Research Center for the growth of ternary and quaternary compounds of indium gallium arsenide (InGaAs) and InGaAsP for LEDs, LDs and detectors. The current trend is away from this type of deposition to metal-organic chemical vapour deposition (MOCVD) which is described a later section.

3.1.2 The study of the InGaAsP LED

The purpose of this part of the study is to find the amount of current spreading that takes place in the LED and to compare the result to the calculation from the current spreading equations presented in the previous sections. If the model is in reasonable agreement with the measured result then it can be used to optimize the layer thicknesses and doping concentrations. A schematic of the LED structure is shown in figure 4.

In order to fabricate an SLD the thicknesses of the layers under the ridge have to be tightly controlled so that little current spreading occurs and a high current density is achieved in the active region. The LED design does not include a ridge and does little to control current spreading under the contact stripe. Figure 4 shows that the p^+ InGaAsP cap layer and the p InP confinement layer are highly doped and relatively thick so a great deal of current spreading is expected.

An LED was taken from a normal production batch and the facet output power recorded for various values of drive current. The emitting region was viewed by a CCD camera through a microscope with a video analyser. A photograph was taken of the image on the monitor. In order to calibrate the camera scale a photograph was also taken of the cleaved end of a 50 μm core fiber.

The characteristics of the LED were calculated, from the equations presented in section 2, using a spreadsheet. This spreadsheet became the basis for all the characterization studies in this report. The details of the LED study are shown in appendix I and the comparison of the measured facet output power and the calculated output power is shown in graph 1.

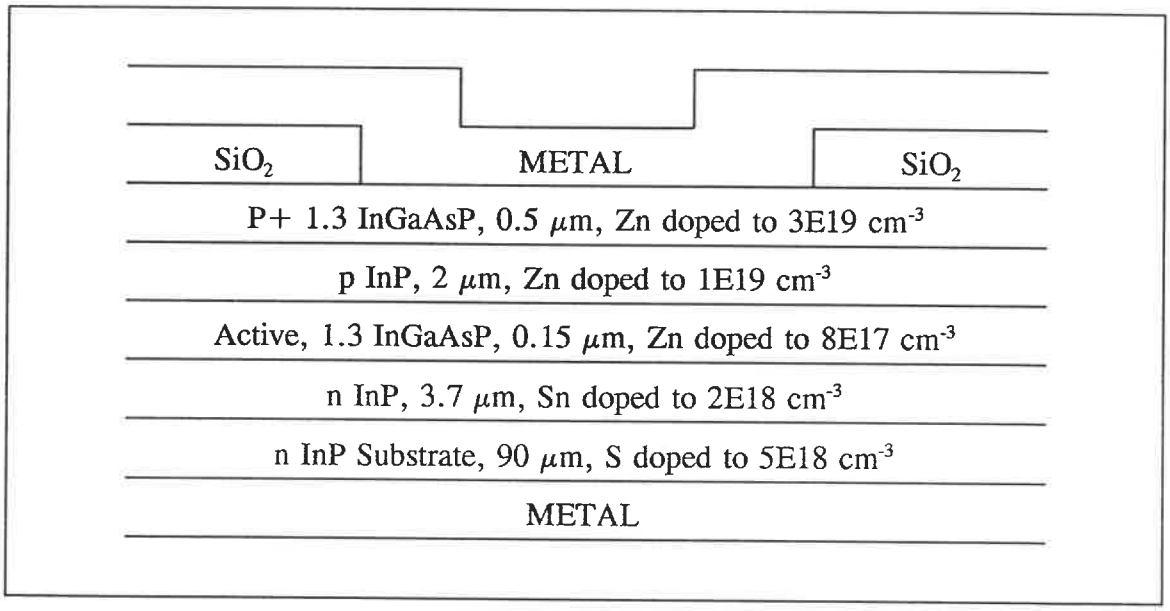

Figure 4 The LED structure used in the study

The results clearly illustrate the need for control of the thickness and doping of the layers. The 6 μm stripe width had expanded to 21 μm at the active region in only 2.5 μm of layer thickness. The calculated emitting length was in good agreement with the measured length. The cap layer needs to be highly doped to make ohmic contact to the evaporated metal and maintain a low voltage drop. The confinement layer is necessary for confining the electrons in the conduction band of the active region, so it would not

be possible to remove or radically change these layers. It was decided that the SLD structure should be grown with an etch-stop layer and an extra InP layer so that a ridge could be formed to reduce the spreading in the highly doped cap layer.

The spectral modulation depth of the LED was not measured, but as this was a normal device the spectrum would be expected to be smooth with less than 1% modulation depth at 150 mA. The LED is manufactured with an 85° angle between facet and stripe in order to reduce the reflection of light back into the cavity and each facet is coated with an anti-reflective layer of scandium oxide.

3.1.3 The study of the SLD grown by VPE

It has been established that the lateral current spreading has to be controlled as much as possible and using a ridge is one means of physically preventing the spread of the current in the cap layer. The ridge can be formed by etching away a part of the layer but it is difficult to control an etch depth with time only; localized heating and bubble formation both cause uneven etching across the wafer. Layer removal can be achieved, in a practical way, by use of an etch-stop layer. In this case the top layer, or cap layer, can be removed with an hydrogen peroxide and sulphuric acid mix and the InP layer can be removed with a 80% HCL and water mix. This last mix will attack the quaternary of the etch-stop only very slowly. In order to allow this approach both an etch-stop layer and an extra InP layer had to be included in the wafer structure.

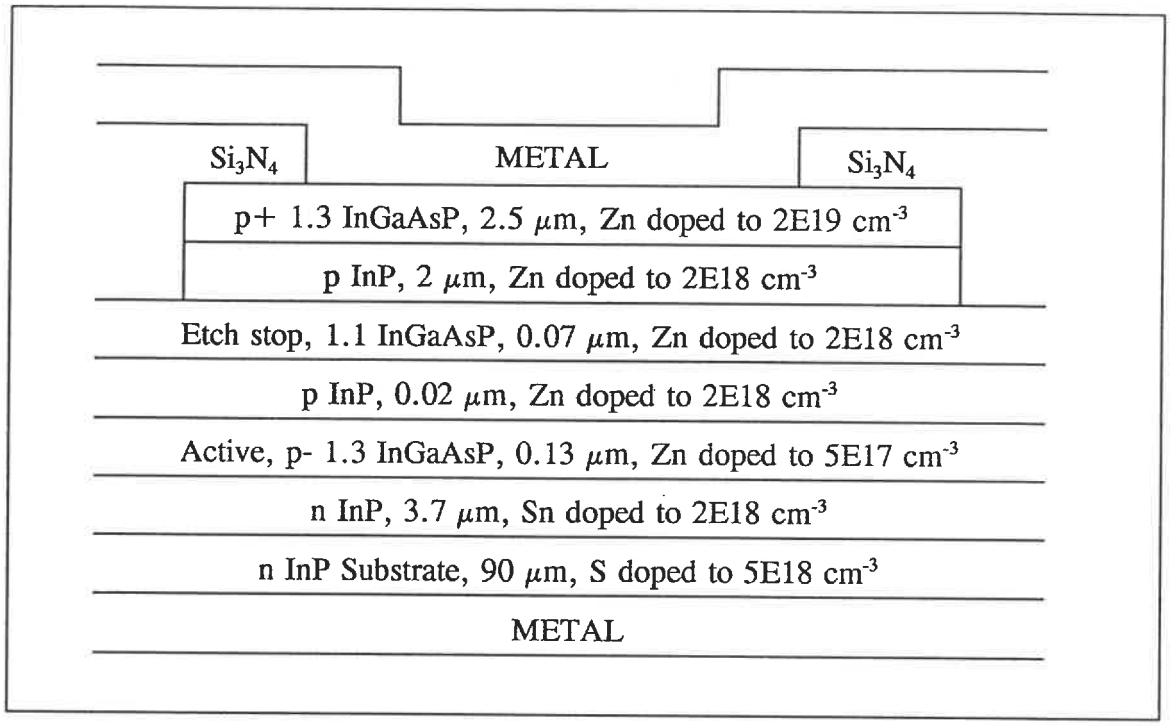

Figure 5 The VPE grown structure used in the study

The layer thicknesses and the doping densities were kept to minimum levels but the layer thicknesses were found to vary by +/- 11.5% across the wafer. This is considered to be normal for a VPE grown wafer and is a weakness of the growth reactor, the external heating causes temperature gradients across the tube and this results in different deposition rates over the diameter of the wafer. It is worth noting at this stage that present-day MOCVD reactors have much better thickness control because the wafers are placed on a heated susceptor which in turn uniformly heats the wafer.

The wafer was characterized by single crystal X-Ray diffractometry, to determine the lattice match between the substrate and grown layers and was found to be matched.

A Polaron C-V plot was made of the grown layers to determine the doping densities. In order to plot deep enough into the wafer the highly doped capping layer was removed by a controlled etch. The thicknesses of the grown layers were determined by scanning electron microscope measurement and the results are included in the spreadsheet calculations. which one?

3.2 DEVICES FROM WAFERS GROWN BY MOCVD

3.2.1 MOCVD growth

In metal-organic chemical vapor deposition thin compound semiconductor films are grown by the reaction of gaseous metal-organic compounds and hydrides at a heated substrate. Since the early eighties this technique has rapidly developed into the main method for the growth of materials for LED and LD manufacture.

Like the VPE process, the solid alloy composition of the deposited layer is determined by the gas composition which is controlled by mass flow controllers. In the MOCVD reactor, the metals are already in a gaseous form and are well mixed. In the VPE process a gas is fed over a heated source, to transfer metals into the vapor, then a mixing process is required. This means that the MOCVD process is capable of depositing layers with more uniform compositions and, because less pipe work is required, there can be a rapid exchange of the gas phase in the reactor allowing sharp interfaces between layers of different compositions. The heated wafer holder can be rotated in the gas flow

to ensure an even thickness of deposited layer and this overcomes the problem of uneven heating in the VPE system.

One application of the MOCVD technique is the preparation of thin compound layers to form strained quantum well and complex multilayer structures. The process can also be used for the deposition of sophisticated III-V structures.

3.2.2 The study of the SLD grown by MOCVD

The VPE growth had never been optimized for low threshold lasers. The broad area threshold current density of the VPE wafer was measured at 7000 A cm^{-3} which is typical of growths for pulsed lasers. At DSRC a Cambridge MOCVD reactor had been modified for growth of low threshold lasers at 1.3 μm and 1.55 μm and, with the co-operation of DSRC personnel, several wafers were grown at 1.3 μm with a similar double heterostructure to the VPE grown wafer. Wafer OM653 was selected for processing because the lattice matching was good and the broad area threshold current was 3751 A cm^{-3}. The details of the structure are shown in figure 6 and there are relatively minor differences in the layers below the ridge when compared to the VPE structure shown in figure 5. The p InP layer is thicker because of a misunderstanding of the exact requirement but this is not considered to be important. The doping levels were deliberately lowered for the MOCVD growth in order to further restrict the current spreading.

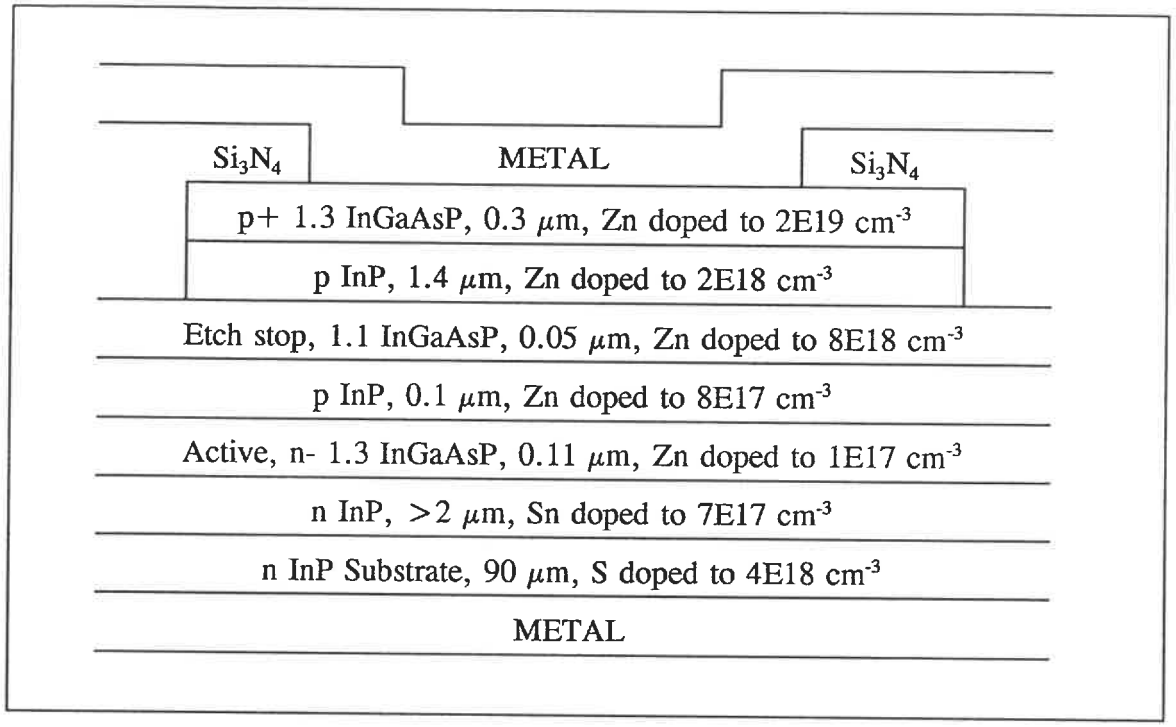

Figure 6 The MOCVD grown structure used in the study

3.3 THE PROCESSING OF THE GROWN WAFERS

3.3.1 The processing flowchart

The wafers were processed using standard EG&G Optoelectronics procedures wherever possible. The following flowchart provides the essential steps of the fabrication process :

1 WAFER PREPARATION :	Lap and polish the wafer and deposit a SiO_2 layer.

2 PHOTORESIST STEP :	Apply the photoresist, align the ridge mask and develop the photoresist.

3 ETCH STEP :	Open the ridges to the etch-stop. Etch the cap with H_2O_2 / H_2SO_4 and etch the InP layer with 80% HCL, then clean off the photoresist.

4 SiO_2 REMOVAL:	Remove the oxide with buffered HF.

5 DEPOSIT Si_3N_4 :	Use the plasma enhanced chemical vapor deposition equipment.

6 PHOTORESIST STEP :	Apply the photoresist and align the stripe mask, then develop the photoresist.

7 ETCH STEP :	Open the stripes in the nitride using reactive ion etching.

8 P CONTACT :	Deposit the AuZn alloy by evaporation, strip of the excess metal and evaporate the P metal onto the surface.

9 N CONTACT :	Evaporate the N metal and treat at high temperature then evaporate another N metal layer.

10 CLEAVE WAFER :	Cleave the wafer into bars and complete a sample evaluation.

11 FACET COAT :	Evaporate scandium oxide anti-reflection coating on both facets.

12 SCRIBE BARS :	Scribe the bars into chips and inspect 100%.

The 80% HCL etch for the InP layer was carried out at 5°C to make the process more controllable. The processing steps are further illustrated in figure 6.

3.3.2 The angled facets and antireflective coatings

The wafer was cleaved into bars at an angle of 85° to the ridge. This is a process used to reduce back reflection into the Fabry-Perot cavity and has been used effectively by EG&G Optoelectronics to prevent low temperature lasing in LEDs. In order to prevent the cavity forming longitudinal modes it is important to reduce the facet to facet reflections in the highly pumped ridge region.

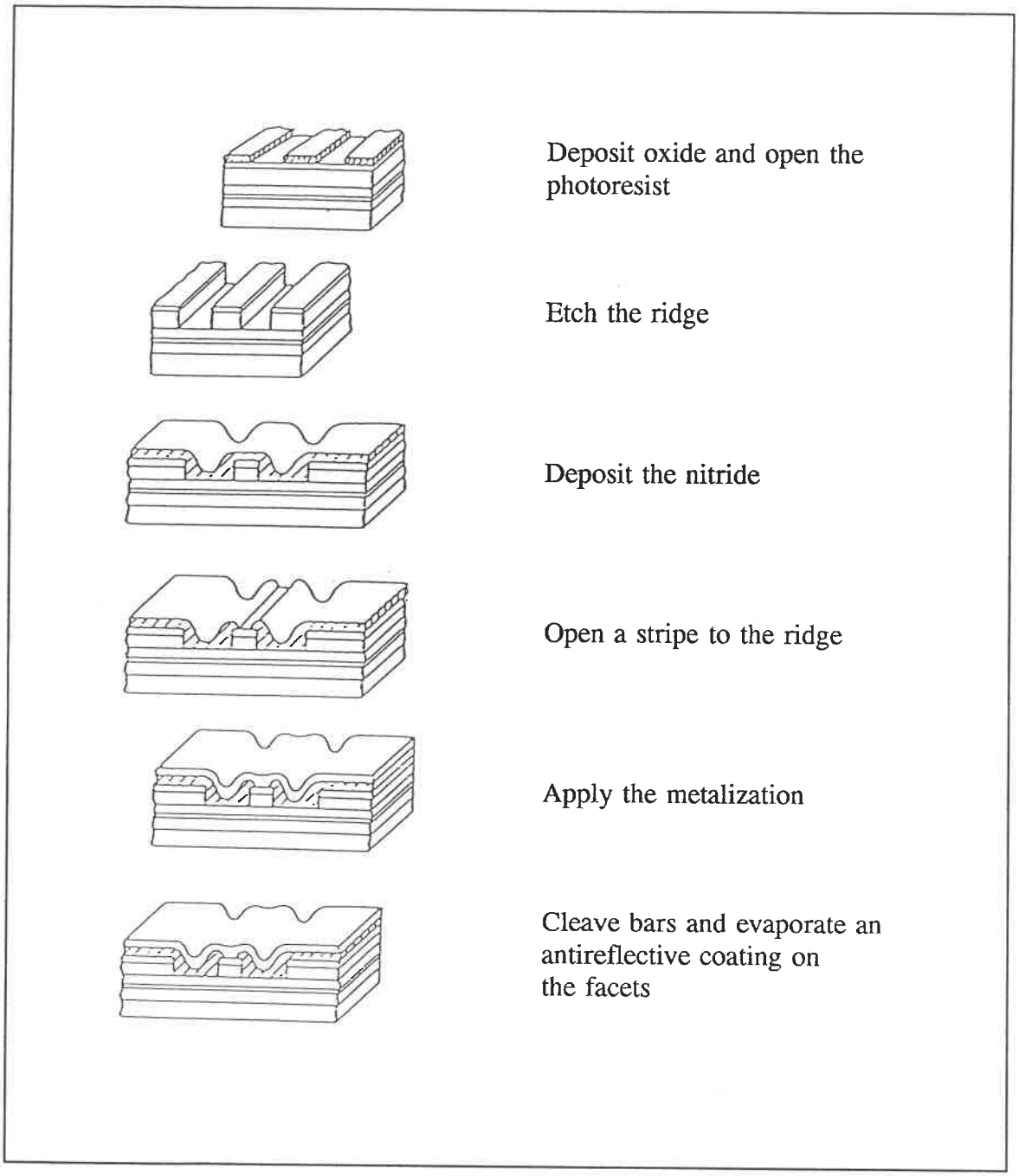

Figure 7 A schematic of the processing steps

The angle needs to be as large as possible to achieve this objective. Unfortunately there is a practical limitation on the maximum angle size, the light emitted from the axis of the ridge is refracted away from the normal. In the case of a 85° cleave angle, the light is emitted at 15° to the normal of the facet.

At a later stage of the manufacturing process, a fiber has to be brought close to the emitting facet and manipulated in all three dimensions to optimize the coupling efficiency. A chip mounted at more than 15° to the axis of the fiber severely reduces the manoeuvrability of the fiber during the alignment process and was for this reason that the 85° cleave angle was chosen for LEDs.

In order to form an effective antireflective coating on the facets of the SLD it is necessary to deposit a single layer quarter-wave film with a refractive index close to 1.8. Electron beam evaporated scandium oxide is ideal for this purpose and has been used extensively by EG&G Optoelectronics on 1.3 μm LEDs.

3.4 THE PACKAGING OF THE CHIPS

3.4.1 The evaluation package

The chip has to be characterized so the results can be compared to the specification. The most important characteristics are the output power and modulation index at various drive conditions. The final section of the theory concluded that a 10 mW

facet output power was required to achieve 1 mW in the fiber. In order to avoid complex fiber alignment, and the introduction of further variables, it was decided to use the facet output, and not the fiber output, to characterize the chip. The chip was evaluated on a coaxial package as shown in figure 8.

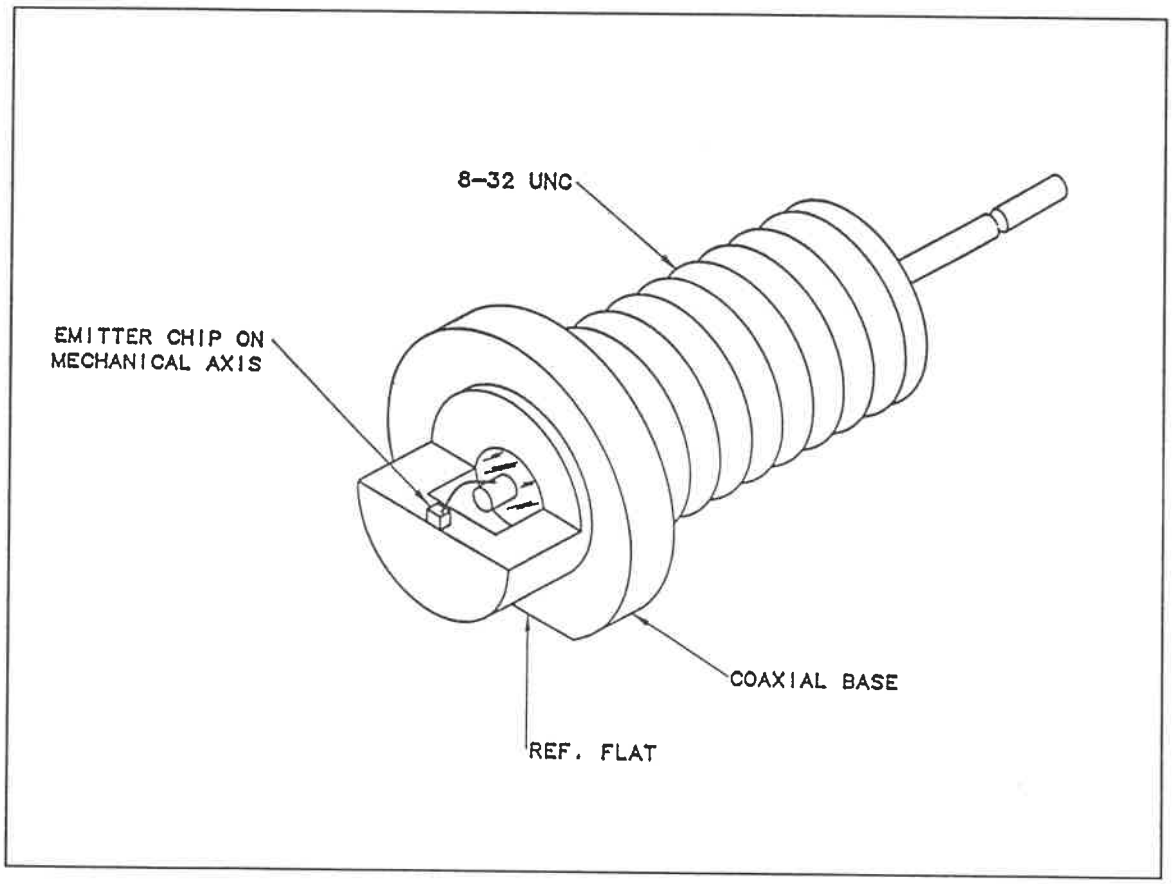

Figure 8 The coaxial package used for facet output power measurements

The chips were soldered on the coaxial package, using standard procedures, then cleaned and inspected. The inspection step was necessary to remove chips that were damaged or had poor optical coatings. This helped to avoid wasting time when the devices were characterized.

The following flowchart provides the essential steps of the assembly process :

1 WELD WIRE : Clean the header and weld 0.002" Au wire to the center lead.

2 SOLDER CHIP : Solder the chip to the package and wire with Pb/Sn solder.

3 CLEAN AND INSPECT : Clean off the flux and inspect the facet for damage.

3.4.2 The final package

The final package is an industry standard 14 pin dual-in-line (DIL) package as shown in figure 9. This design has been used by EG&G Optoelectronics to manufacture short wavelength SLDs with polarization maintaining fiber. At 0.85 μm the core diameter of the single mode fiber is less than the core diameter of single mode fiber at 1.3 μm. The package is fully hermetic, a cover is welded to the top of the shell and the finished product is leak tested to the military standard.

A monitor photodiode is aligned to the rear facet of the SLD chip. The output of the photodiode is used to provide feedback to the current drive in order to achieve constant output power. The surface of the photodiode is reflective to some extent and care must be taken to avoid reflected light entering the SLD chip.

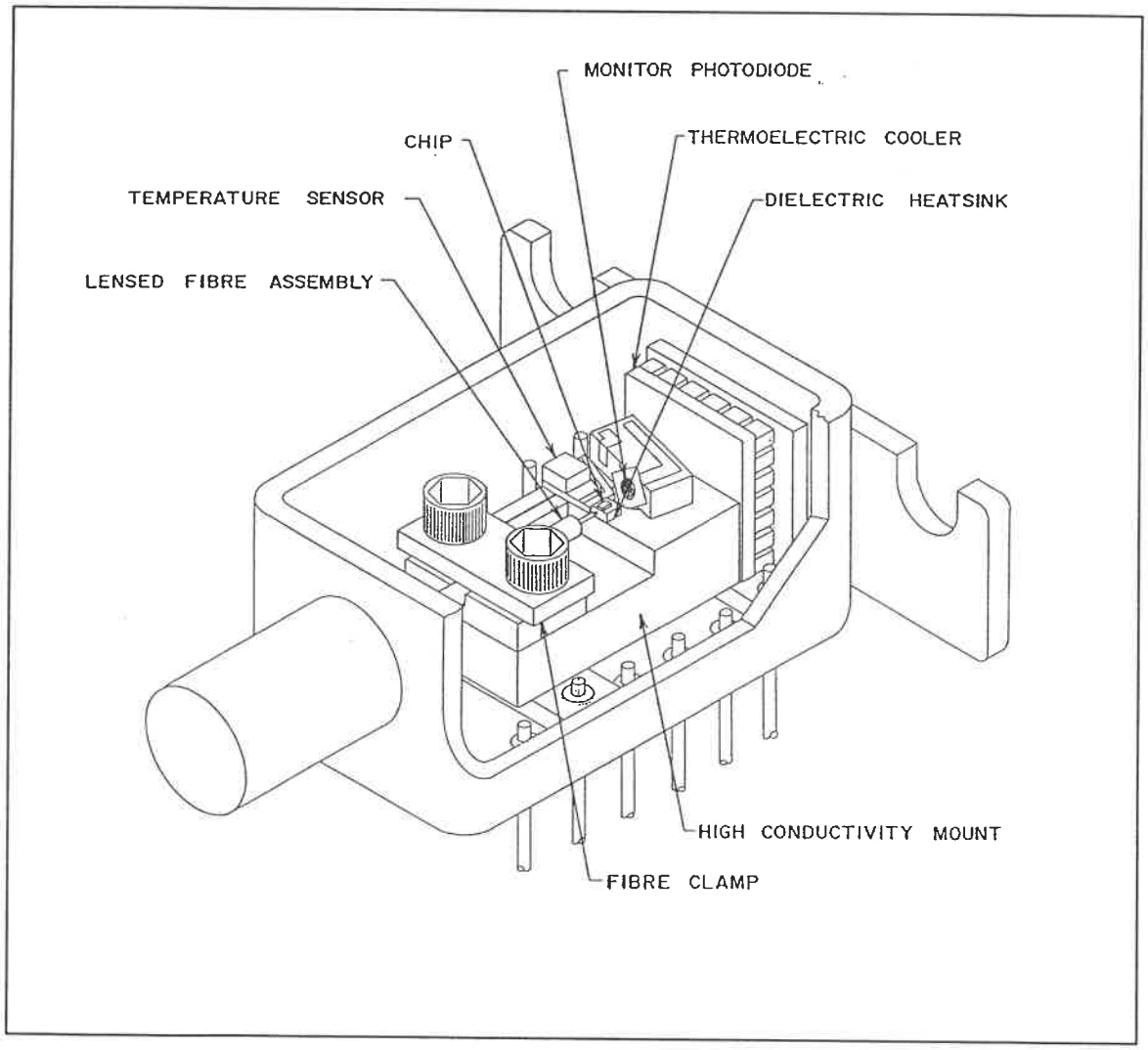

Figure 9 The 14 pin DIL package

The following flowchart provides the major steps of the assembly process:

1 MOUNT CHIP AND WIRE BOND :	Solder the chip onto a submount and wire bond. Clean and inspect the chip for facet damage.
2 TEST AND BURN IN :	Test the output power and burn-in the submount.
3 ASSEMBLE COOLER IN DIL :	Solder the cooler in place then clean and inspect for damage.
4 PREPARE FIBER :	Solder the fiber into a tube with Au/Sn solder then clean and inspect for damage.
5 ASSEMBLE THERMISTOR :	Solder the thermistor on the submount then clean and wire bond.
6 DIL ASSEMBLY :	Assemble the submount assembly and align and fix the fiber assembly.

7 ASSEMBLE PHOTODIODE :	Fix the photodiode onto ceramic mount with epoxy and wire bond to the pad. Test and inspect for damage.

8 ASSEMBLE PHOTODIODE IN DIL :	Fix the assembly onto the submount and wire bond to the pins.

9 SEAM SEAL :	Weld a cover on the package and test for leaks.

10 ADD HEATSHRINK AND MARK :	Add the heatshrink for fiber support. Mark the covers using permanent ink.

11 FINAL TEST :	Test output power and wavelength at several temperatures. Check the cooler, thermistor and monitor photodiode.

The fabrication steps are shown in detail in appendix X and appendix XI. No 1.3 μm SLDs were made in this package but the details are included here for costing purposes. The specification has the requirement for a device that will maintain a constant chip temperature while the ambient varies between 10°C and 40°C. A thermistor and thermoelectric cooler are included in the package for this purpose. The coaxial mount

does not accommodate a cooler nor is it a suitable package for accurately holding a fiber. The 14 pin DIL package, on the other hand, has already demonstrated this capability and is known to survive thermal cycling between the storage temperatures of 0°C to 75°C.

SECTION 4

RESULTS

4.1 GENERAL

A specification, developed from a market survey of devices required for optical amplifiers and fiber optic gyroscopes, is presented in section 1 of this report.

Twenty five devices were manufactured and were characterized for comparison to the specification. Five devices were made from a VPE grown wafer and twenty devices were made from an MOCVD grown wafer. None of the devices made the required output power at the specified drive current limit and the devices, that were tested for wavelength, failed the specification for modulation depth.

The equations, presented in section 2 of this report, were used in a spreadsheet to calculate the variation of the facet output power and modulation depth with drive current. Wherever possible measured values were used in the equations and the remaining values were obtained from the literature. The internal quantum efficiency and, in some cases, the current spreading width were calculated and related to direct measurement. The optical efficiency, defined as the probability of a spontaneously generated photon exiting one facet of the chip, and the gain coefficient were varied to obtain the best fit to the actual results. The fit to the modulation depth was obtained by

varying the reflection coefficient of the facets.

4.2 THE RESULTS FROM THE STUDY OF THE LED STRUCTURE

EG&G Optoelectronics routinely grows wafers to support a high power, 1.3 μm, LED requirement. The first approach to developing the superluminescent diode was to use wafers from this program. The spreadsheet study, based on the characteristics of the LEDs, was performed with a typical value for the Auger coefficient. The optical efficiency and gain coefficient were used as variables to fit the output power curve.

Drive current, mA	Calculated output power, mW	Actual output power, mW
200	0.70	0.70
180	0.58	0.59
160	0.48	0.49
140	0.38	0.39
120	0.30	0.30
100	0.22	0.22
80	0.16	0.15
60	0.10	0.10
40	0.05	0.05
20	0.02	0.02
0	0.00	0.00

Table 1 The results of the study of the LED

The fit of the output power was accomplished with an optical efficiency of 1.6% and a gain coefficient of 1.77×10^{-16} cm^2 and the modulation depth was calculated with a reflection coefficient of 0.002 to agree with an estimated 1% modulation depth for the LEDs in current production.

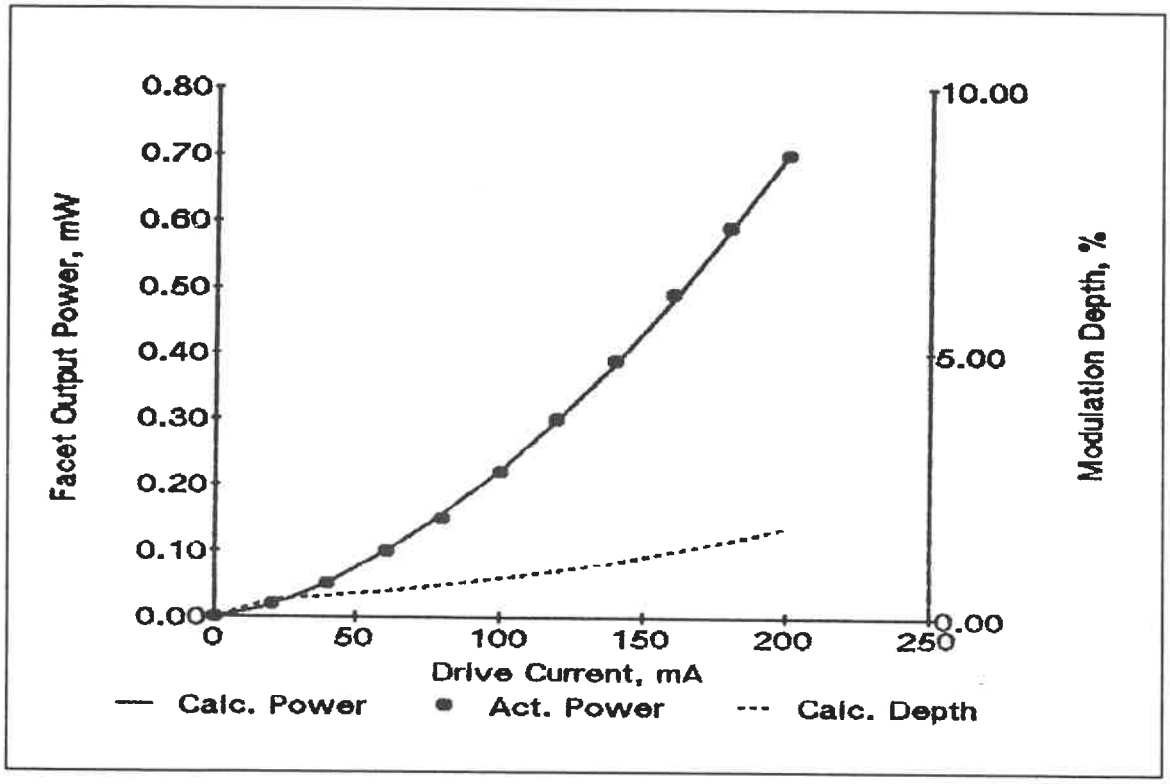

Graph 1 The comparison of calculated and actual results for the LED

The spreadsheet results are shown in appendix I. In order to check the calculation of the current spreading a photograph of the emitting facet was taken and the length of the emitting region was measured and compared to the calculated value. This photograph

is shown in photograph 1 and a photograph of a 50 μm fiber, which was used for calibration, is shown in appendix IX.

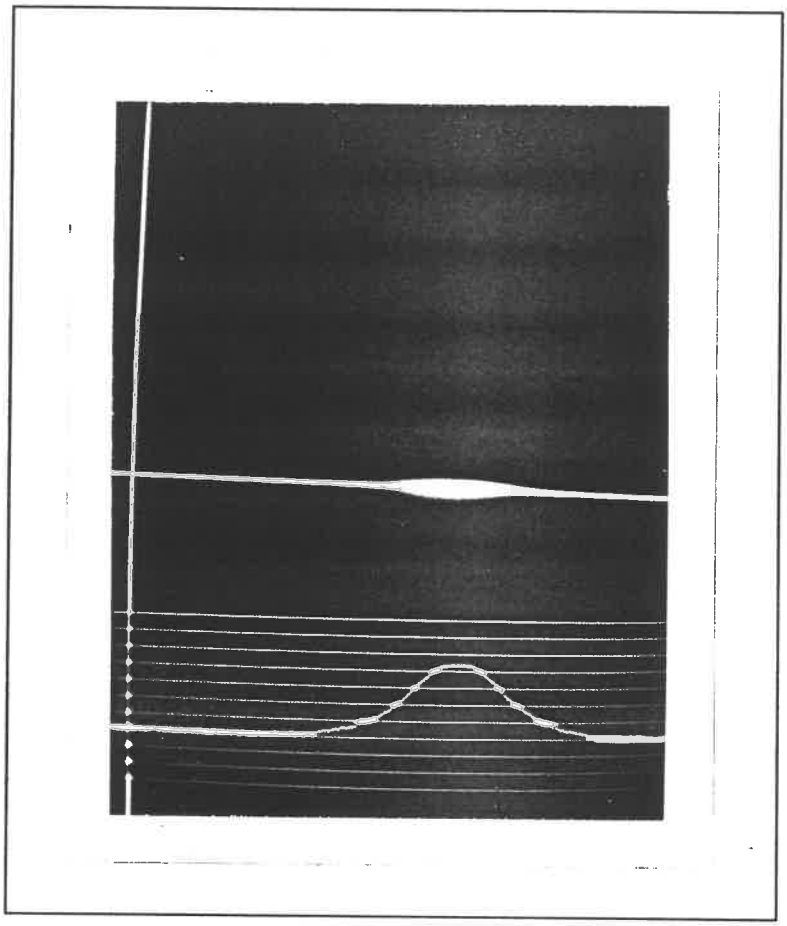

Photograph 1 The photograph of the emitting facet of the LED

The results were in agreement, the measured value of the emitting length was 22 μm and the calculated value was 21.5 μm, at 150 mA.

4.3 THE RESULTS FROM THE STUDY OF THE VPE GROWN DEVICES

4.3.1 The results from A1159#M5

A wafer was grown by VPE with the structure shown in figure 5. The wafer was processed with a ridge in order to reduce current spreading in the highly doped cap layer and achieve a high current density at the active region.

Drive current, mA	Calculated output power, mW	Actual output power, mW	Calculated modulation depth, %	Actual modulation depth, %
300	7.14	7.30	25.51	24.0
280	5.51	5.40	19.86	
260	4.18	4.00	15.26	16.8
240	3.10	2.93	11.45	
220	2.26	2.16	8.50	
200	1.64	1.60	6.26	7.3
180	1.14	1.17	4.47	2.7
160	0.8	0.84	3.21	
140	0.54	0.60	2.22	
120	0.35	0.42	1.49	
100	0.23	0.27	0.99	
80	0.14	0.17	0.63	
60	0.08	0.07	0.39	
40	0.05	0.01	0.22	
20	0.02	0.00	0.12	
0	0.00	0.00	0.00	0.0

Table 2 The results of the study of A1159#M5

Five devices were made and were characterized to varying degrees. One of the two best devices, A1159#M5, had superluminescent characteristics. The output power versus drive current curve, shown in graph 2, is typical of a superluminescent diode, the threshold knee, common in laser diodes, is absent. The spectral plot, shown in graph 3, confirms superluminescent operation. The spectral width is of the order of 60 nm and the envelope is showing signs of modulation.

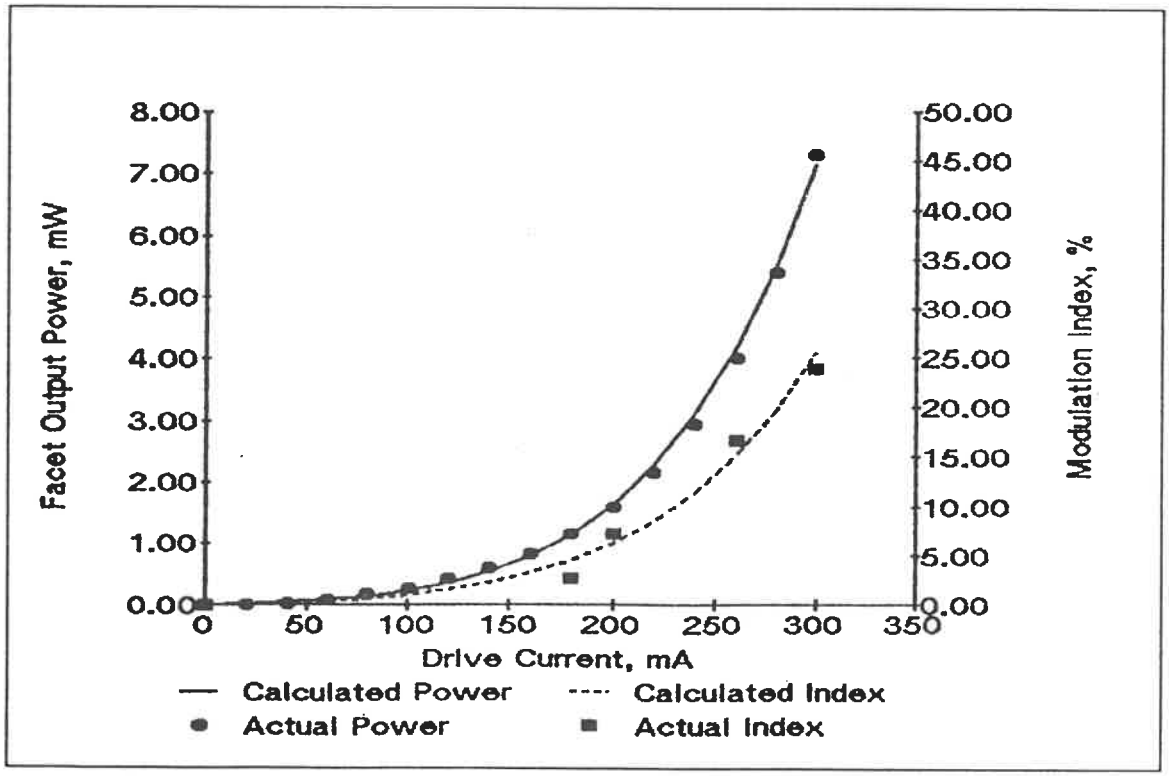

Graph 2 The comparison of calculated and actual results for A1159#M5

In this case, the spreadsheet study used values of 0.36% for the optical efficiency and 2.07×10^{-16} cm^2 for the gain coefficient. A good fit between the calculated and actual power results was achieved. A reflection coefficient of 0.0012 was used to compare the calculated and actual modulation depth results. Calculating the modulation depth from the spectral plot is difficult because of the irregular nature of the curve but, nevertheless, a reasonable agreement between the calculated and actual results is shown in graph 2.

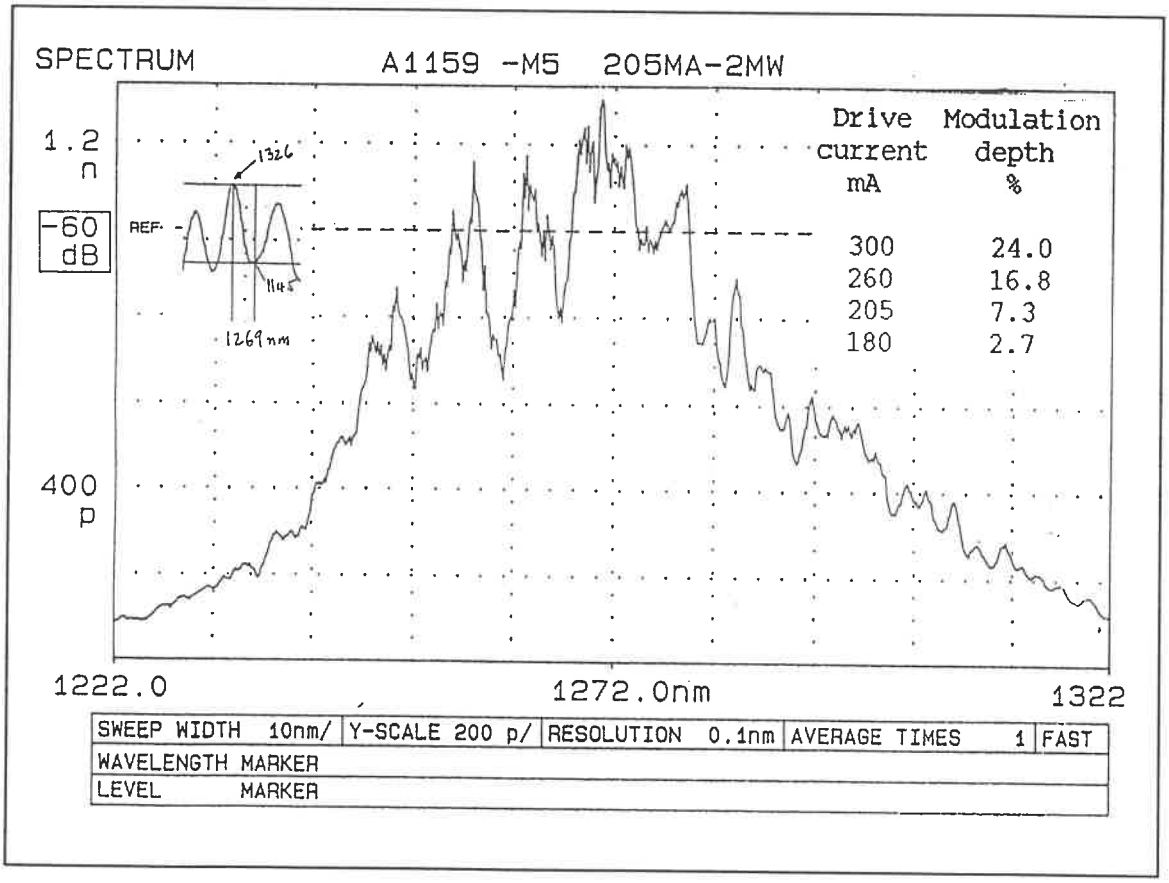

Graph 3 The spectral plot of A1159#M5

The spectral plot was the only plotted result, the modulation depths for the other power levels were calculated directly from the interferometer. The peak to valley reading was measured directly with the aid of a reference cursor.

4.2.2 The results from A1159#M7 and A1159#M3

Drive current, mA	A1159#M7 Calculated output power, mW	A1159#M7 Actual output power, mW	A1159#M3 Calculated output power ,mW	A1159#M3 Actual output power, mW
300	20.78		0.43	0.43
280	15.00		0.45	0.44
260	10.65		0.44	0.44
240	7.31	7.50	0.41	0.44
220	4.93	5.00	0.36	0.43
200	3.28	3.00	0.31	0.40
180	2.12	1.90	0.26	0.39
160	1.33	1.23	0.21	0.37
140	0.80	0.80	0.16	0.30
120	0.46	0.51	0.12	0.24
100	0.27	0.31	0.09	0.19
80	0.14	0.17	0.06	0.10
60	0.08	0.06	0.04	0.02
40	0.04	0.00	0.02	0.00
20	0.02	0.00	0.01	0.00
0	0.00	0.00	0.00	0.00

Table 3 The results of the study of A1159#M3 and A1159#M7

A1159#M7 displayed a superluminescent type of output power characteristic but A1159#M3 looked like a poor LED. A1159#M7 had a similar optical efficiency and gain coefficient to A1159#M5 but A1159#M3 required an optical efficiency of 0.17% and a gain coefficient of 1.4×10^{-16} cm^2 to achieve a fit between the calculated and actual results.

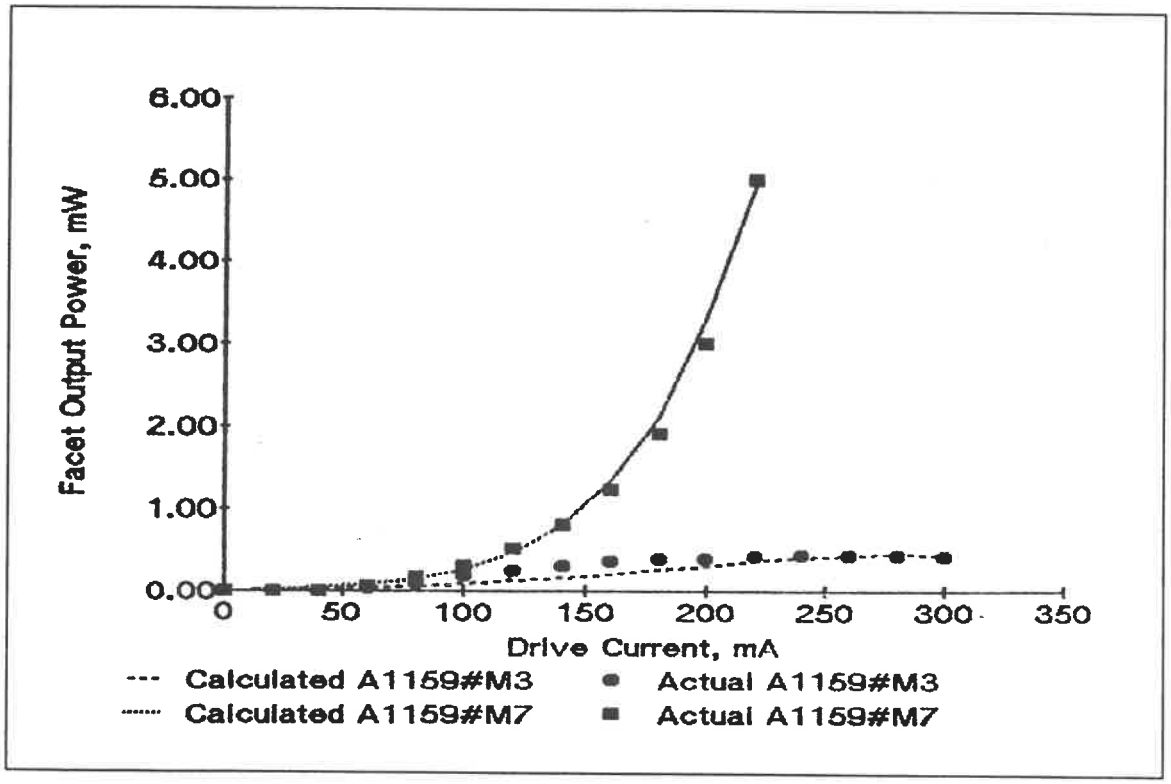

Graph 4 The comparison of actual and calculated results for A1159#M3 and A1159#M7

The spreadsheets are shown in appendix III and appendix IV. Graph 4 is intended to show the best and worse output power results from the VPE wafer. The worse device required lower values of optical efficiency, gain coefficient and spontaneous radiative coefficient to account for the difference. This suggests that there was a growth related problem with this device, possibly the interfaces were of poor quality and reduced the carrier and optical confinements. The low value of optical efficiency suggests poor processing but this was not apparent through an optical microscope. The calculated modulation depth for A1159#M7 was in good agreement with the measured values when a reflection coefficient of 0.0012 was used.

The threshold current density of wafer A1159 was measured as 7000 A cm^{-2}. This translates into an internal quantum efficiency of 10.1% and both the best devices fitted the power output curves with internal quantum efficiencies of 10%. In order to fit the worse device to the power output curve the spontaneous radiative coefficient was lowered and reduced the internal quantum efficiency to 5.1%.

4.4 THE RESULTS FROM THE STUDY OF THE MOCVD GROWN DEVICES

4.4.1 The results from OM653#3 and OM653#9

A wafer was grown by MOCVD, with the structure shown in figure 6, and was processed in the same way as the VPE wafer. The results were surprising because the MOCVD grown devices did not show signs of superluminescence. OM653#9 and

OM653#3 are the best and the worse devices and the results are displayed in table 4 and graph 5 and the spreadsheet results are shown in appendix V and appendix VI.

Drive current, mA	OM653#3 Calculated output power, mW	OM653#3 Actual output power, mW	OM653#9 Calculated output power ,mW	OM653#9 Actual output power, mW
200	0.12	0.12	0.30	0.30
180	0.11	0.11	0.27	0.27
160	0.10	0.10	0.23	0.23
140	0.09	0.09	0.20	0.20
120	0.08	0.08	0.16	0.17
100	0.07	0.07	0.13	0.14
480	0.06	0.06	0.10	0.11
60	0.04	0.04	0.08	0.08
40	0.03	0.03	0.05	0.06
20	0.02	0.02	0.03	0.03
0	0.00	0.00	0.00	0.00

Table 4 The results of the study of OM653#3 and OM653#9

For the spreadsheet analysis, the worse device required a lower optical efficiency value, a lower spontaneous radiative coefficient value and a higher Auger coefficient value than the best device. In fact the worse VPE grown device was better then the best MOCVD grown device. OM653#9 required an optical efficiency of 0.35% and a gain coefficient of 1.2×10^{-16} cm^2. This suggests that the MOCVD wafer was well processed but poorly grown.

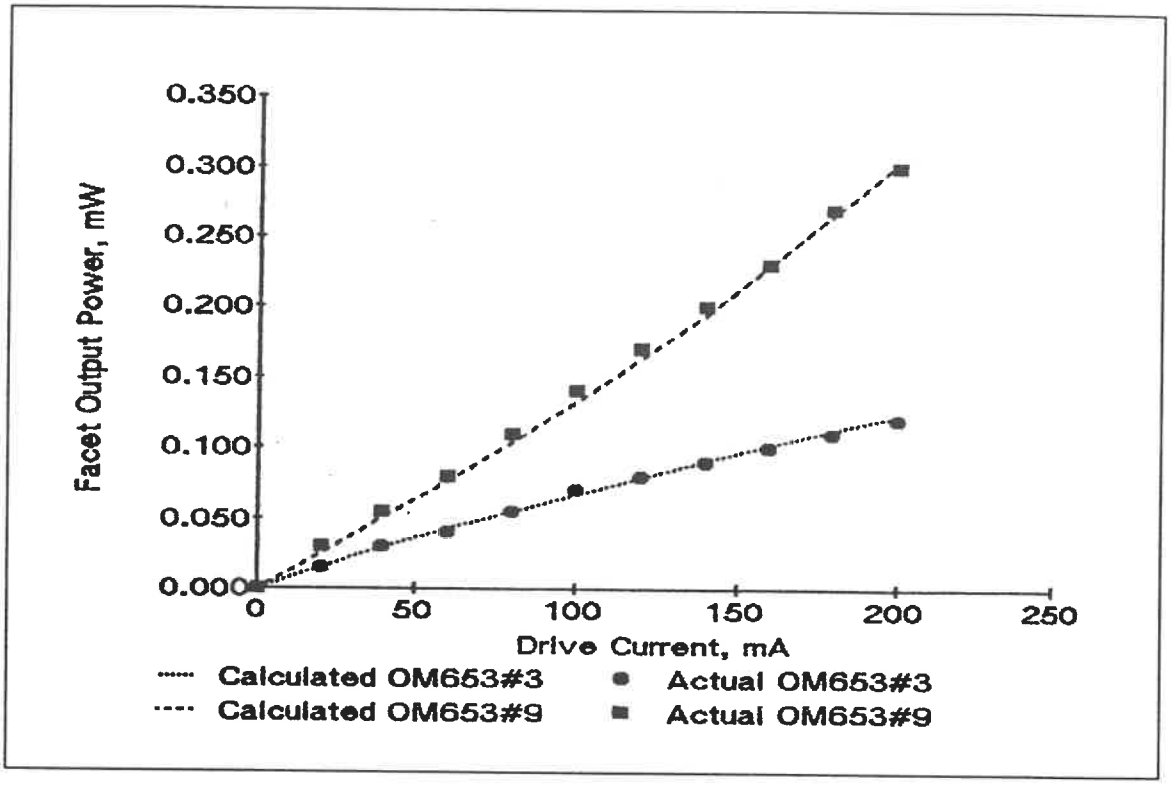

Graph 5 The comparison of actual and calculated results for OM653#3 and OM563#9

The broad area threshold current density of wafer OM653 was measured as 3751 A cm^{-2}. This indicated that the material was of reasonable quality and translates into an internal quantum efficiency of 18.1%. The best device fitted the power output curve with an internal quantum efficiency of 14.3%. This difference is probably caused by non-uniform layer thicknesses across the wafer, especially across the active region. The gain coefficient was lower for the MOCVD devices than the VPE devices and this suggests poor optical confinement because of poor interfaces between the layers and, probably, this is the main reason for the devices not having superluminescent

characteristics.

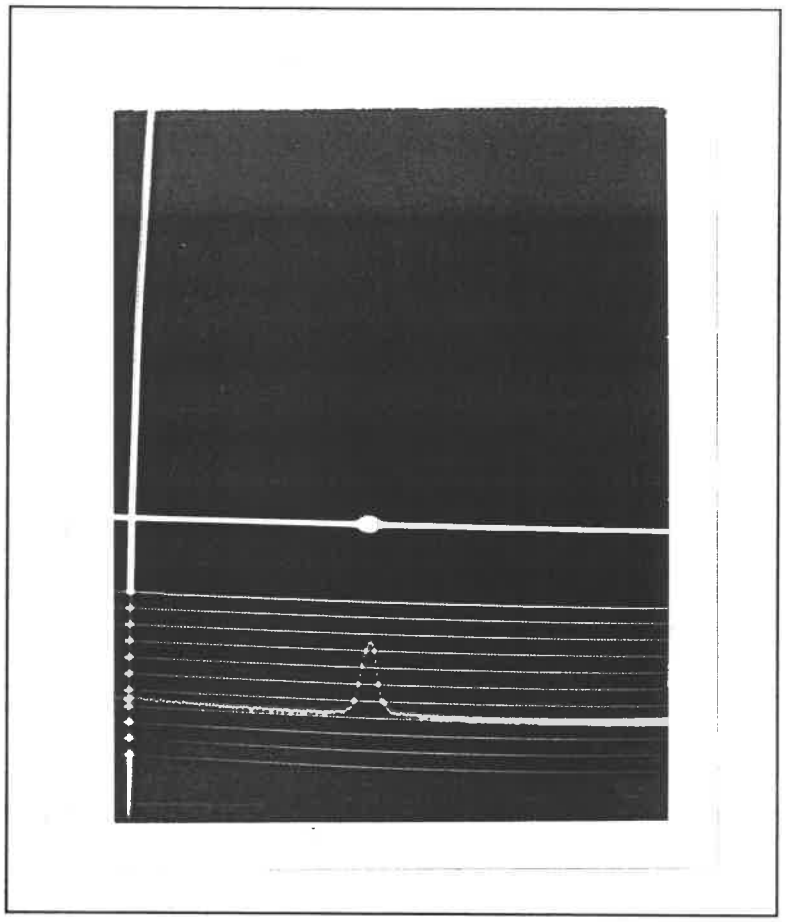

Photograph 2 The photograph of the emitting facet of OM653#3

There was concern, initially, that the ridges were poor on these devices even though they looked normal under an optical microscope. The active region width of OM653#3 was photographed in the same way as the LED. The result is shown in

photograph 2. The emitting length of 8.3 μm compares well with the calculated value of 8.51 μm, at 100 mA, and suggests that the wafer has been well processed. This is supported by the relatively high optical efficiency for both devices.

4.5 THE RESULTS FROM THE SPREADSHEET ANALYSIS

4.5.1 The selection of values for the analysis

The objective of this analysis is to optimize the output power and find the value of the reflection coefficient that gives a modulation depth of less than 10%. The first step is to select values for the parameterss that were not measured.

Parameter	A1159#M5	A1159#M7	OM653#9	Optimistic value
Optical loss, cm^{-1}	30	30	30	30
Optical efficiency, %	0.36	0.3	0.35	0.4
Radiative constant, cm^3s^{-1}	7×10^{-11}	7×10^{-11}	7×10^{-11}	7×10^{-11}
Radiative ratio	1.7×10^{-19}	1.7×10^{-19}	1.7×10^{-19}	1.7×10^{-19}
Auger coefficient, cm^6s^{-1}	8×10^{-29}	8×10^{-29}	7×10^{-29}	7×10^{-29}
Gain coefficient, cm^2	2.07×10^{-16}	2.5×10^{-16}	1.2×10^{-16}	2.5×10^{-16}
Transparency density, cm^{-3}	1.5×10^{18}	1.5×10^{18}	1.5×10^{18}	1.5×10^{18}

Table 5 The comparison of the values from the best devices and the values selected for the optimistic analysis

The carrier mobility values, for the three layers below the ridge, were kept the same through all the studies and a 0.4% value for the optical efficiency was selected from an optimistic view of the results obtained. The other parameters, shown in table 5, were selected as the best values obtained from devices in this report. The selected values for the radiative constant and the radiative ratio are the limit values shown by Agrawal and Dutta[1].

The second step of the analysis is to select the values of the measured parameters. The current spreading results for OM653#3 show that the emitting length is the same as the fiber core diameter. This is a reasonable condition for launching light into a single mode fiber. Therefore, it was decided not to change the thicknesses of the cladding layer, the thickness of the etch-stop, the doping concentrations or the ridge dimensions.

4.5.2 The results from the analysis

The selected values were placed in the spreadsheet and several iterations were made with different variables. The cavity length and the active region thickness were found to be important variables. The results show that the maximum output power is achieved with an active layer thickness of 0.22 μm and the modulation depth will not exceed the maximum specified value if the reflection coefficient is less than 0.0004.

Active Region Thickness, μm	Maximum Output Power, at 150 mA, mW	Maximum Modulation Depth at 150 mA, %
0.10	1.8	2.7
0.11	2.4	3.4
0.12	3.0	4.2
0.13	3.6	5.2
0.14	4.2	6.0
0.15	4.8	6.9
0.16	5.4	7.8
0.17	5.9	8.4
0.18	6.3	9.1
0.19	6.6	9.4
0.20	6.8	9.7
0.21	6.9	9.8
0.22	7.0	9.9
0.23	7.0	10.0
0.24	6.9	9.8
0.25	6.8	9.6
0.26	6.7	9.2
0.27	6.5	8.9
0.28	6.2	8.3
0.29	5.9	7.8
0.30	5.6	7.2

Table 6 The variation of output power and modulation depth with active region thickness

An active layer thickness of 0.22 μm was used for the rest of the analysis. This suggests that the VPE and MOCVD structures were grown with an inadequate active layer thickness. Once the active region thickness was fixed the effect of cavity length was

explored. A cavity length of 500 μm had been used on the devices made from the VPE and MOCVD wafers because it was the standard cavity length for LEDs made by EG&G Optoelectronics.

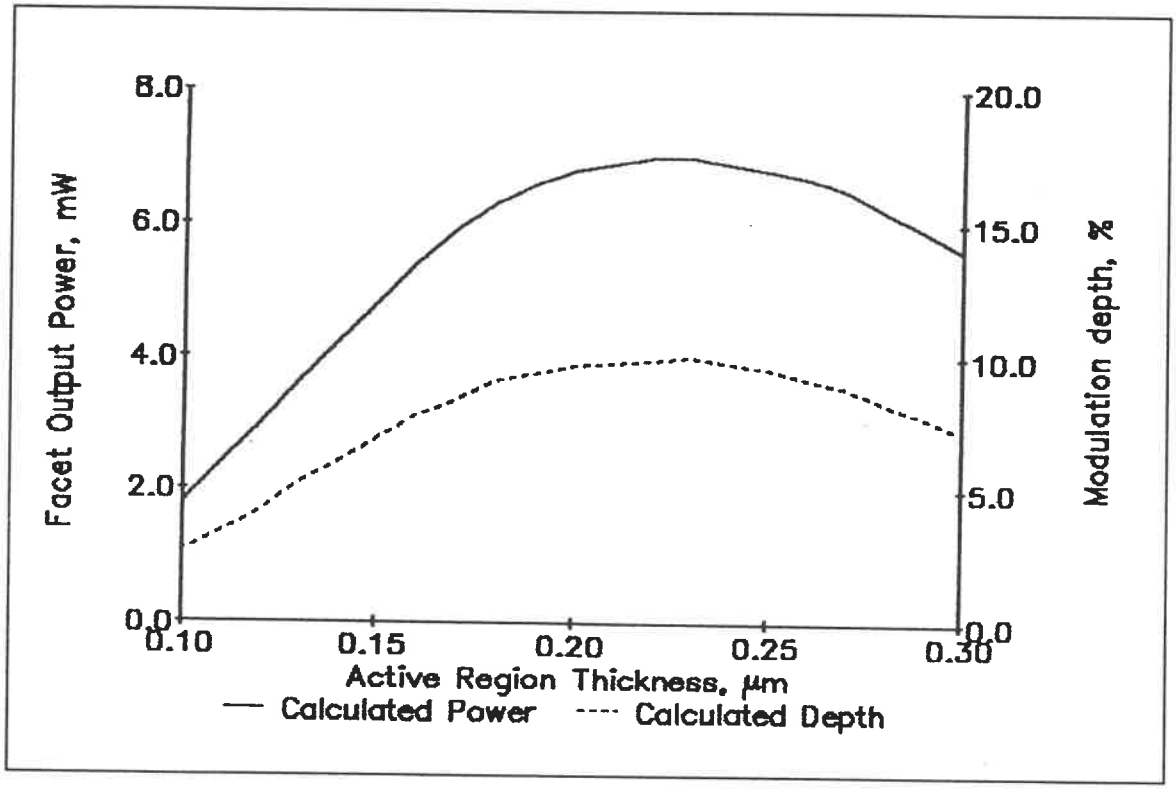

Graph 6 The variation of output power and modulation depth with active region thickness

The spreadsheet was rearranged and the cavity length analysis was carried out at 150 mA. The results show a maximum output power of 7.08 mW with a cavity length of 500 μm and a drive current of 150 mA. The maximum modulation depth occurs at 400

μm although the difference between 400 μm and 500 μm is small. This result supports the use of 500 μm cavity lengths for 1.3 μm LEDs but the optimum cavity length may vary with active layer thickness.

Cavity length, μm	Calculated output power, mW (150 mA)	Calculated output power, mW (160 mA)	Calculated modulation depth, % (150 mA)	Calculated modulation depth, % (160 mA)
200	2.08	2.54	5.11	4.15
300	4.50	6.09	8.20	7.27
400	6.47	9.29	9.91	9.26
500	7.08	10.81	9.63	9.53
600	6.60	10.15	8.20	8.18
700	5.11	8.38	5.92	6.29
800	3.70	6.14	4.03	4.34
900	2.41	4.17	2.47	2.79
1000	1.59	2.69	1.52	1.70
1100	0.97	1.74	0.85	1.03
1200	0.64	0.66	0.50	0.58
1300	0.41	0.45	0.27	0.32
1400	0.30	0.33	0.16	0.18
1500	0.24	0.25	0.10	0.11
1600	0.21	2.54	0.07	0.07

Table 7 The variation of output power and modulation depth with cavity length and drive current

This analysis does predict that it is possible to fabricate an SLD with a fiber output power greater than 1 mW if a 16% coupling efficiency is assumed. This is

unlikely in a production environment and a 10% coupling efficiency is considered to be more realistic, in which case, the facet output power must exceed 10 mW.

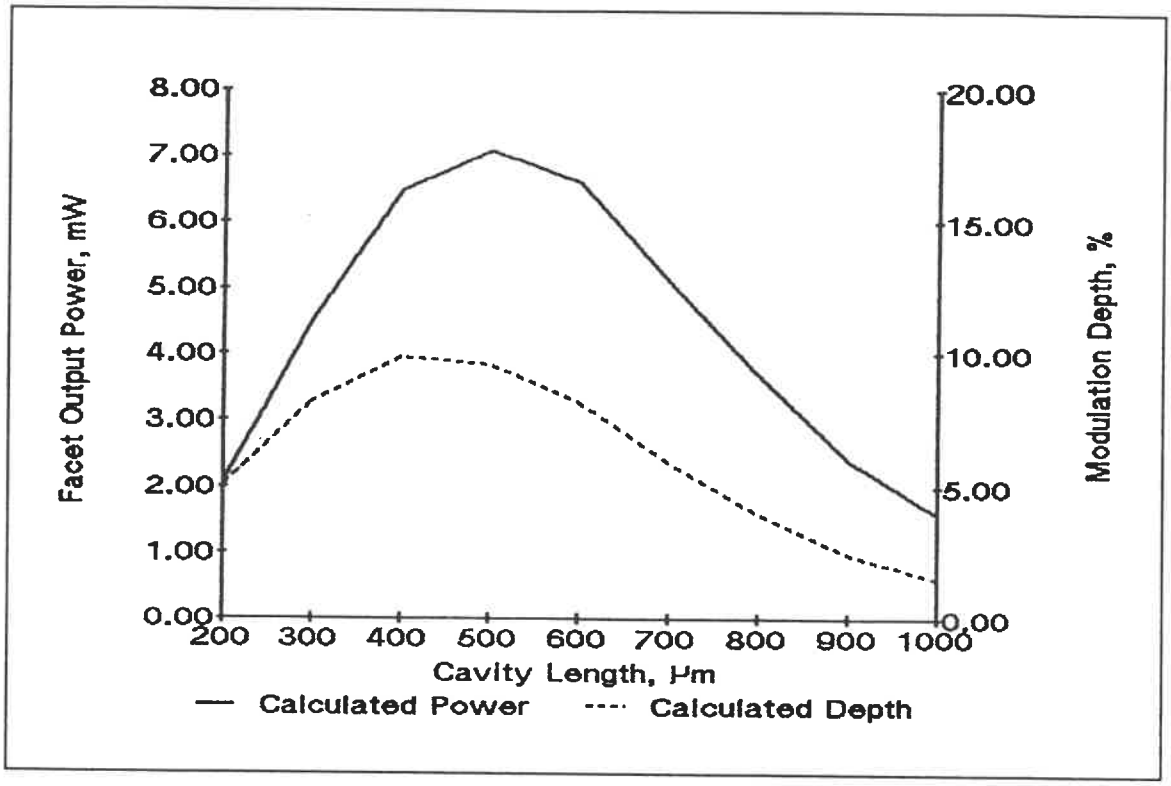

Graph 7 The output power and modulation depth predictions with a drive current of 150 mA and a reflection coefficient of 0.0006

The analysis was repeated at 160 mA to see if a marginal increase in drive current could achieve this power level. At this drive current, the analysis predicts that an SLD, made with a cavity length of 500 μm, an active layer thickness of 0.22 μm and a

reflection coefficient of less than 0.0004 will conform to the specification for output power and modulation depth. The detailed results can be seen in appendix VIII.

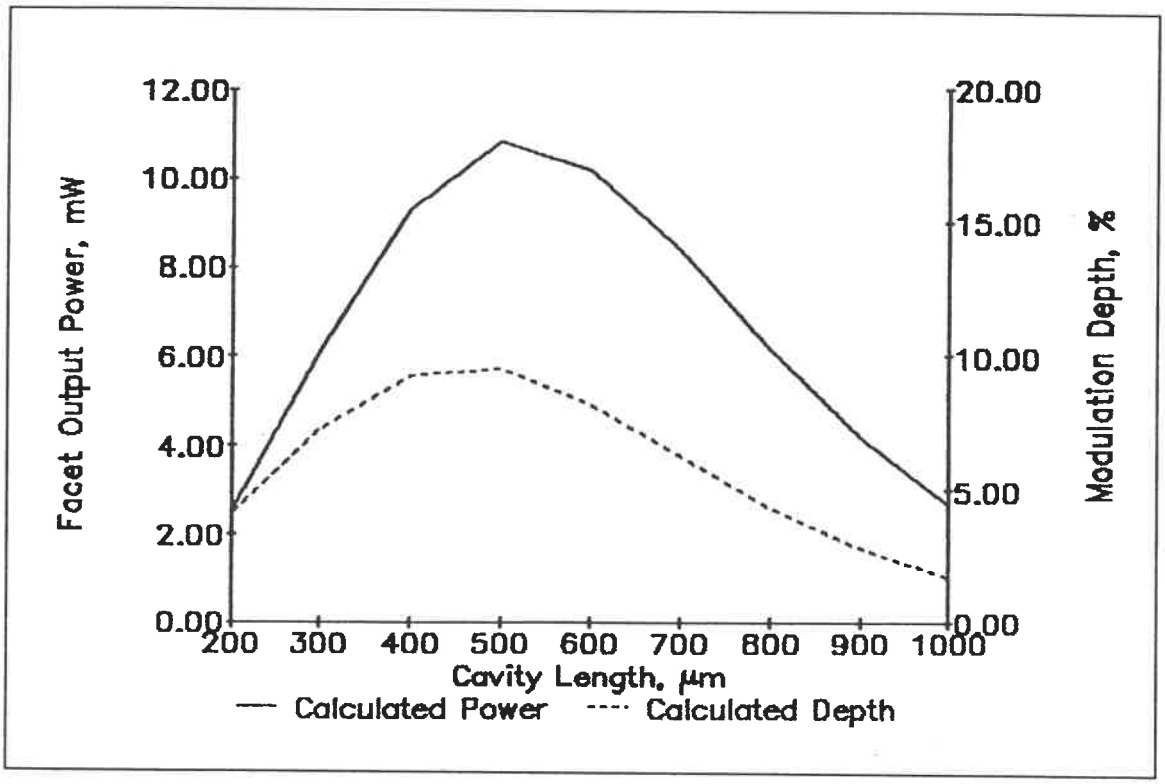

Graph 8 The output power and modulation depth predictions with a drive current of 160 mA and a reflection coefficient of 0.0004

The best reported results[8] give a facet output power of 10 mW, with a current drive of 175 mA, and a modulation depth of 15%. The chip, in this case, consists of a pump region and an end-absorbing region to prevent reflection. An index-guided buried crescent structure, grown partly by MOCVD and partly by liquid phase epitaxy, is used

for this device. The cavity length is 730 μm, typically, with a 300 μm absorber region.

4.6 THE RESULTS OF THE COSTING STUDY

The whole manufacturing process was built up in two parts, firstly the material costs and, secondly, the routing costs. Actual material costs were used except where there were high quantities. Then the cost reduction was estimated. Wherever possible, actual process times were used for the routing and where times were unknown, the times were estimated against a similar process. The major difficulty was in estimating the yields. Two options were studied, first, a best cost option where the assembly yield was taken as 66% and the wafer yield was taken as 1 in 2. These yield levels are currently being achieved on a production line for LEDs. Secondly, a worse case option where the assembly yield was taken as 50% and the wafer yield as 1 in 10.

Quantity per annum	**1**	**10**	**100**	**1000**	**10000**
Best cost option, $	2979	904	571	484	428
Worse cost option, $	12826	1906	765	631	560

Table 8 The results of the cost study showing the unit cost

Labour and overhead rates were not those specifically in use at EG&G Optoelectronics because that information is company private but competitive rates, considered to be normal for this type of business, were used.

The details of the costing structures are contained in appendix X and appendix XI. The costing is constructed with the material costs first then the labor costs on a step by step basis. The sequence number, in the first column of the material costing, refers to the routing step that uses the material. The factor, in the third column, indicates the yield expectation. The best cost option, in table 8, shows that it is possible to fabricate SLDs for less than $500 in quantities of 1000 or more.

SECTION 5

DISCUSSION

5.1 GENERAL

The key parts of the specification are the output power and modulation depth and none of the devices, in this report, gave results that approached the specified values. Even with optimistic values in the model the output power predictions were marginal. In this section the results from the device characterization work and the results from the theory are discussed. The costing exercise showed that it was possible to manufacture devices for less than $500 each and a possible cost saving opportunity is presented. The last subject to be discussed is the potential of alternate materials which are currently being investigated.

5.2 THE OUTPUT POWER

The results were disappointing, only two devices had characteristics that showed superluminescence and both were from the VPE wafer. The theory presented in this report is not precise or extensive but the values used for the parameters are within the limits quoted by the literature and the theory did allow the modelling of the best and the worse devices. The theory did predict the current spreading and the internal quantum efficiency with reasonable agreement.

The study of the variation of output power with cavity length, for drive currents of 150 mA and 160 mA, was based on the best values seen in the study of the actual devices. If the optical efficiency and the Auger coefficient values were applied to the best device, A1159#M7, the output power would increase from 1.0 mW to 2.02 mW. The change in active layer thickness, from 0.13 μm to 0.22 μm, would produce a further increase of the output power to 4.3 mW, at 150 mA. It would still require the drive current to increase to 160 mA for the output power to reach 10 mW.

The main problem with the InGaAsP active layer is the relatively high value of the Auger recombination coefficient. This reduces the internal quantum efficiency because a high proportion of the carriers are recombining nonradiatively. An Auger coefficient of 4×10^{-29} cm^6 s^{-1} applied to the spreadsheet for A1159#M7 without any other changes, would give a facet output power of 10.3 mW. This value of Auger coefficient is inside the range quoted by Agrawal and Dutta[1] but it is suggested, in this reference, that p doped InGaAsP is likely to have a higher coefficient. A material with an Auger coefficient of less than 2×10^{-29} cm^6 s^{-1} would be desirable.

5.3 THE MODULATION DEPTH

The calculated reflection coefficient was compared to actual results for the device A1159#M5. The modulation depth was found to increase quickly when gain started and a reflection coefficient of much less than 0.001, per facet, would be required to suppress

modulation. A quick modification to the spreadsheet for A1159#M5 showed that a reflection coefficient of 0.0004 per facet would be required to maintain a modulation depth of less than 10% at 300 mA. This result is confirmed by graph 8 which shows a reflection coefficient of 0.0004 to maintain a 10% modulation depth at 10 mW.

Increasing the active later thickness to 0.22 μm has another advantage. The SLD is diffraction limited in the direction perpendicular to the active layer and, from equation (38), the angular divergence is inversely proportional to the active layer thickness. A thicker active region would allow more light to be coupled into the fiber.

The facet to facet reflections can be reduced by use of a good antireflective coating. Electron-beam evaporated films of scandium oxide have given reflection coefficients of 2.5×10^{-4} per facet[9] and this is the technology currently in use at EG&G Optoelectronics. However, it is difficult to control the thickness and refractive index of the optical coating and this could be improved by depositing by a sputtering technique. Sputtering equipment is expensive and there is a possibility of damaging the facet during the deposition process.

The angled stripe geometry attempts to dissipate the reflected light in the plane of the active region. A possible improvement on this would be to dissipate the reflected light in the substrate, away from the active region[7]. In order to achieve this effect an angled facet would have to be etched or milled into the plane of the active region and

would introduce further processing steps and consequently increase the cost of the chip. There would have to be a beneficial yield improvement in achieving the modulation index to make this approach worthwhile.

The David Sarnoff Research Center staff proposed another approach with the use of low-pumped, gain guided regions at the facets. These end regions would allow the reflected light to more easily escape into the non-pumped areas beyond the ridge. This technique, however, still maintains the light in the plane of the active region.

5.4 THE COSTING STUDY

The yield factors are responsible for a large proportion of the total cost. The accuracy can only be confirmed by fabricating a substantial number of devices.

The thermoelectric cooler and the thermistor account for $70 to $100 of the cost. If close wavelength control is not required then it would be possible to make a cheaper device. A different package outline could be used if a cooler and thermistor are not included. The CD player, laser package is cheap and several companies have developed fibering techniques for this type of package.

5.5 ALTERNATE MATERIALS

The work being carried out on strained materials is relevant to the superluminescent diode. Although a narrow active region thickness has been used as the structure in this development, it could be possible to make SLDs from multiple quantum well devices. If this is the case, the quantum wells could be made of strained InGaAs. There is extensive research being done in this area and values of the Auger coefficient and gain coefficient should soon be available in the literature.

CONCLUSION

The specification for a 1.3 μm superluminescent diode is outlined in section 1 of this report. The specification is not achievable with InGaAsP as an active region material. The output power may be achieved at 160 mA but the yield of wafers with the right parameters will be small unless considerable engineering work is carried out in some fundamental areas of growth and processing. Even then, the high value of the Auger coefficient severely reduces the chances of this material making the baseline specification. None of the devices, made from the material grown and processed in this report, made the specification for output power.

The modulation index of 10% is achievable with a reflection coefficient of 0.0004 but the technology currently available to EG&G Optoelectronics only demonstrated a reflection coefficient of 0.001. Again, further engineering work would be required along some of the promising options discussed in this report.

The packaging of very small core, polarisation maintaining fiber has been demonstrated at EG&G Optoelectronics for SLDs at 820 nm. A costing estimation based on this device showed that a cost of less than $500, per unit, would only be possible with a very high yield (1 in 2 good wafers and a 66% overall assembly yield). This applies only to quantities greater than 1000 per annum.

The new strained material now being investigated for telecommunications devices is looking promising for SLD structures. This material is expected to have a lower Auger recombination coefficient and a higher internal quantum efficiency. Because the InGaAsP material has a marginal power performance which could lead to a low and erratic yields, it would be prudent to continue this development with strained InGaAs material and to return to InGaAsP only if the development does not succeed.

RECOMMENDATIONS

1. Investigate strained materials to see if the Auger coefficient is lower than 2×10^{-29} cm^6 s^{-1}. There are other important parameters associated with the material and the spreadsheet model, presented in this report, can be used to evaluate them.

2. Investigate putting an angled facet in the plane of the active region in order to reduce the reflection coefficient to less than 0.04%.

3. For future development work, adopt the yield guidelines shown in this report. The cost of the SLD will exceed $500 unless the wafer yield is better than 1 in 2 and the assembly yield is better than 66%.

REFERENCES

[1] AGRAWAL G. P. and DUTTA N. K., 1986 "Long-wavelength Semiconductor Lasers". 1st edition, Van Nostrand Reinhold Company, New York, NY.

[2] BOTEZ D., April 1978 "Analytical Approximation of the Radiation Confinement Factor for the TE_0 Mode of a DoubleHeterojunction Laser". IEEE Journal of Quantum Electronics, Vol QE-14, 230-232.

[3] CASEY H. C. and PANISH M. B., 1978 "Heterostructure Lasers - Part B: Materials and Operating Characteristics". 1st edition, Academic Press, Orlando, Florida.

[4] DUTTA N. K., January 1981 "Gain-Current Relation for $In_{0.72}$ $Ga_{0.28}$ $As_{0.6}$ $P_{0.4}$ Lasers". Journal of Applied Physics 52(1), 55-60.

[5] FIELDER F. and SCHACHETZKI A., 1987 " Optical Parameters of InP Based Waveguides", Solid State Electronics Vol 30, No. 1, 73-83.

[6] HENRY C., March 1986 "Theory of Spontaneous Emission Noise in Open Resonators and its Application to Lasers and Optical Amplifiers". Journal of Lightwave Technology, Vol LT-4, No. 3, 288-297.

[7] JANSEN et al., January 1990 "Superluminescent diode". US Patent Number 4896195.

[8] KWONG N.S.K, BAR-CHAIM N. and CHEN T., January 1989 "High-powered 1.3μm superluminescent diode". Applied Physics Letters 54(4), 298-300.

[9] LADANY I., ZANZUCCHI J., ANDREWS J., KANE J. and DEPIANO E., September 1985 "Scandium Oxide Anti-reflection Coatings for Superluminescent LEDs". RCA Lab. Technical Report, PRRL-85-TR-128.

[10] PEARSALL T.P. (Editor), 1982 "GaInAsP Alloy Semiconductors". 1st edition, John Wiley & Sons, New York, NY.

[11] THOMPSON G. H. B., 1980 "Physics of Semiconductor Laser Physics". 1st edition, John Wiley & Sons, New York, NY.

APPENDIX I: The spreadsheet study of the LED

Measured values :

Doping level of layer 1 :	3E+19	atoms cm^-3
Doping level of layer 2 :	1E+19	atoms cm^-3
Doping level of the active region :	8E+17	atoms cm^-3
Thickness of layer 1 :	0.5	µm
Thickness of layer 2 :	2	µm
Thickness of the active layer :	0.15	µm
Stripe width :	6	µm
Cavity length :	180	µm
Half width of the near field at 150 mA :	22	µm
Wavelength :	1.27	µm

Assumed values :

Mobility in layer 1 :	50	cm^2 V^-1 s^-1
Mobility in layer 2 :	70	cm^2 V^-1 s^-1
Mobility in the active layer :	70	cm^2 V^-1 s^-1
Optical losses :	30	cm^-1
Optical efficiency :	1.6	%
Radiative constant :	7E-11	cm^3 s^-1
Radiative ratio :	1.7E-19	
Auger coefficient :	5E-29	cm^6 s^-1
Gain coefficient :	1.77E-16	cm^2
Transparency density :	9E+17	atoms cm^-3
Reflection coefficient :	0.002	

APPENDIX I (continued)

Calculations :

B(n) cm^3 s^-1	Ja A cm^-2	Io mA	Is mA	Lo cm	2xSy+w µm	ni	D
3.18E-11	4756	74.39	200.1	8.69E-04	16.99	0.165	1.052
3.42E-11	4016	68.36	180.1	9.46E-04	18.49	0.185	
3.67E-11	3324	62.20	160.3	1.04E-03	20.32	0.208	------
3.94E-11	2662	55.65	140.1	1.16E-03	22.71	0.235	1/Rs
4.24E-11	2046	48.80	119.7	1.32E-03	25.91	0.268	ohm^-1
4.55E-11	1512	41.95	100.2	1.54E-03	30.13	0.306	
4.91E-11	1019	34.43	79.9	1.88E-03	36.71	0.358	0.035
5.29E-11	621	26.89	60.5	2.40E-03	47.01	0.423	
5.75E-11	292	18.42	40.0	3.51E-03	68.61	0.522	
6.29E-11	80	9.66	20.2	6.69E-03	130.82	0.677	

g cm^-1	Gs	Gsm	Psp µW	P mW	Gmax	Gmin	M %
4.09E+02	1.1E+01	4.3E+00	1.33E+02	6.99E-01	4.34E+00	4.19E+00	1.71
3.73E+02	9.1E+00	3.7E+00	1.26E+02	5.84E-01	3.71E+00	3.60E+00	1.46
3.36E+02	7.1E+00	3.1E+00	1.17E+02	4.81E-01	3.16E+00	3.08E+00	1.25
2.96E+02	5.5E+00	2.6E+00	1.06E+02	3.84E-01	2.67E+00	2.61E+00	1.06
2.51E+02	4.1E+00	2.2E+00	9.25E+01	2.97E-01	2.23E+00	2.19E+00	0.88
2.05E+02	3.1E+00	1.8E+00	7.83E+01	2.23E-01	1.86E+00	1.83E+00	0.74
1.52E+02	2.2E+00	1.5E+00	6.16E+01	1.55E-01	1.53E+00	1.51E+00	0.61
9.56E+01	1.5E+00	1.2E+00	4.44E+01	9.97E-02	1.25E+00	1.24E+00	0.50
2.67E+01	9.8E-01	9.9E-01	2.57E+01	5.12E-02	9.94E-01	9.86E-01	0.40

APPENDIX I (continued)

Calculated results :

Resistivity of layer 1 :	0.0042 ohms cm
Resistivity of layer 2 :	0.0089 ohms cm
Resistivity of the active layer :	0.1116 ohms cm
Sheet resistivity of the 3 layers :	29 ohms
Confinement factor :	0.356
Half width of the near field at 150 mA :	21.5 µm
Internal quantum eff. at 4016 A cm^-2 :	18.5 %

Carrier Density cm^-3	Spontaneous Coefficient cm^3 s^-1	Drive Current mA	Output Power mW	Emitting Length µm	Modulation Depth %	Actual Power mW
3.21E+18	3.18E-11	200	0.70	16.99	1.71	0.70
3.01E+18	3.42E-11	180	0.58	18.49	1.46	0.59
2.80E+18	3.67E-11	160	0.48	20.32	1.25	0.49
2.57E+18	3.94E-11	140	0.38	22.71	1.06	0.39
2.32E+18	4.24E-11	120	0.30	25.91	0.88	0.30
2.06E+18	4.55E-11	100	0.22	30.13	0.74	0.22
1.76E+18	4.91E-11	80	0.16	36.71	0.61	0.15
1.44E+18	5.29E-11	60	0.10	47.01	0.50	0.10
1.05E+18	5.75E-11	40	0.05	68.61	0.40	0.05
6.00E+17	6.29E-11	20	0.02	130.82	0.31	0.02

APPENDIX II: The spreadsheet study of A1159#M5

Measured values :

Doping level of layer 3 :	2E+18	atoms cm^-3
Doping level of layer 4 :	2E+18	atoms cm^-3
Doping level of the active region :	5E+17	atoms cm^-3
Thickness of layer 3 :	0.07	µm
Thickness of layer 4 :	0.02	µm
Thickness of the active layer :	0.13	µm
Ridge width :	5	µm
Cavity length :	500	µm
Broad area threshold current density :	7000	A cm^-2
Wavelength :	1.27	µm

Assumed values :

Mobility in layer 3 :	60	cm^2 V^-1 s^-1
Mobility in layer 4 :	80	cm^2 V^-1 s^-1
Mobility in the active layer :	73	cm^2 V^-1 s^-1
Optical losses :	30	cm^-1
Radiative constant :	7E-11	cm^3 s^-1
Radiative ratio :	1.7E-19	
Auger coefficient :	8E-29	cm^6 s^-1
Optical efficiency :	0.36	%
Gain coefficient :	2.07E-16	cm^2
Transparency density :	1.5E+18	atoms cm^-3
Reflection coefficient :	0.0012	

APPENDIX II (continued)

Calculations :

B(n) cm^3 s^-1	Ja A cm^-2	Io mA	Is mA	Lo cm	2xSy+w µm	ni	D
2.47E-11	9911	25.96	299.7	5.24E-05	8.98	0.075	0.912
2.59E-11	9203	25.01	280.1	5.44E-05	8.94	0.080	
2.72E-11	8496	24.03	260.5	5.66E-05	8.89	0.086	-----
2.85E-11	7764	22.98	240.0	5.92E-05	8.84	0.093	1/Rs
3.00E-11	7046	21.89	219.9	6.21E-05	8.79	0.100	ohm^-1
3.14E-11	6346	20.77	200.2	6.55E-05	8.72	0.108	
3.31E-11	5619	19.55	179.6	6.96E-05	8.64	0.118	3E-04
3.48E-11	4949	18.34	160.4	7.41E-05	8.55	0.128	
3.67E-11	4251	17.00	140.3	8.00E-05	8.44	0.141	
3.88E-11	3547	15.53	119.7	8.76E-05	8.29	0.156	
4.11E-11	2892	14.02	100.4	9.70E-05	8.10	0.174	
4.38E-11	2213	12.27	79.9	1.11E-04	7.83	0.199	
4.69E-11	1582	10.37	60.3	1.31E-04	7.44	0.232	
5.10E-11	953	8.05	39.9	1.69E-04	6.70	0.285	
5.66E-11	390	5.15	20.1	2.64E-04	5.16	0.385	

g cm^-1	Gs	Gsm	Psp µW	Po mW	Gmax	Gmin	M %
4.77E+02	7.1E+02	1.1E+02	6.55E+01	7.14E+00	1.43E+02	8.47E+01	25.51
4.56E+02	5.2E+02	8.4E+01	6.51E+01	5.51E+00	1.03E+02	6.90E+01	19.86
4.35E+02	3.8E+02	6.4E+01	6.44E+01	4.18E+00	7.50E+01	5.52E+01	15.26
4.11E+02	2.7E+02	4.8E+01	6.34E+01	3.10E+00	5.39E+01	4.28E+01	11.45
3.86E+02	1.9E+02	3.5E+01	6.21E+01	2.26E+00	3.87E+01	3.26E+01	8.50
3.60E+02	1.3E+02	2.6E+01	6.04E+01	1.64E+00	2.78E+01	2.45E+01	6.26
3.31E+02	8.3E+01	1.9E+01	5.82E+01	1.14E+00	1.95E+01	1.78E+01	4.47
3.02E+02	5.4E+01	1.3E+01	5.58E+01	8.02E-01	1.38E+01	1.30E+01	3.21
2.69E+02	3.3E+01	9.3E+00	5.26E+01	5.40E-01	9.46E+00	9.05E+00	2.22
2.32E+02	1.9E+01	6.2E+00	4.88E+01	3.51E-01	6.29E+00	6.11E+00	1.49
1.93E+02	1.1E+01	4.1E+00	4.44E+01	2.28E-01	4.18E+00	4.10E+00	0.99
1.45E+02	5.4E+00	2.6E+00	3.88E+01	1.40E-01	2.63E+00	2.59E+00	0.63
9.11E+01	2.5E+00	1.6E+00	3.23E+01	8.46E-02	1.63E+00	1.61E+00	0.39
2.07E+01	8.7E-01	9.3E-01	2.39E+01	4.62E-02	9.37E-01	9.33E-01	0.22
-7.66E+01	2.1E-01	5.1E-01	1.32E+01	1.99E-02	5.06E-01	5.05E-01	0.12

APPENDIX II (continued)

Calculated results :

Resistivity of layer 3 :	0.0521 ohms cm
Resistivity of layer 4 :	0.0391 ohms cm
Resistivity of the active layer :	0.1712 ohms cm
Sheet resistivity of the 3 layers :	3824 ohms
Confinement factor :	0.294
Broad area internal quantum efficiency :	10.1 %
Internal quantum eff. at 7046 A cm^-2 :	10.0 %

Carrier Density cm^-3	Spontaneous Coefficient cm^3 s^-1	Drive Current mA	Output Power mW	Modulation Depth %	Actual Power mW	Actual Modulation Depth, %
3.81E+18	2.47E-11	300	7.14	25.51	7.30	24.0
3.71E+18	2.59E-11	280	5.51	19.86	5.40	
3.60E+18	2.72E-11	260	4.18	15.26	4.00	16.8
3.49E+18	2.85E-11	240	3.10	11.45	2.93	
3.37E+18	3.00E-11	220	2.26	8.50	2.16	
3.24E+18	3.14E-11	200	1.64	6.26	1.60	7.3
3.10E+18	3.31E-11	180	1.14	4.47	1.17	2.7
2.96E+18	3.48E-11	160	0.80	3.21	0.84	
2.80E+18	3.67E-11	140	0.54	2.22	0.60	
2.62E+18	3.88E-11	120	0.35	1.49	0.42	
2.43E+18	4.11E-11	100	0.23	0.99	0.27	
2.20E+18	4.38E-11	80	0.14	0.63	0.17	
1.94E+18	4.69E-11	60	0.08	0.39	0.07	
1.60E+18	5.10E-11	40	0.05	0.22	0.01	
1.13E+18	5.66E-11	20	0.02	0.12	0.00	

APPENDIX III: The spreadsheet study of A1159#M7

Measured values :

Doping level of layer 3 :	2E+18	atoms cm^-3
Doping level of layer 4 :	2E+18	atoms cm^-3
Doping level of the active region :	5E+17	atoms cm^-3
Thickness of layer 3 :	0.07	µm
Thickness of layer 4 :	0.02	µm
Thickness of the active layer :	0.13	µm
Ridge width :	5	µm
Cavity length :	500	µm
Broad area threshold current density :	7000	A cm^-2
Wavelength :	1.27	µm

Assumed values :

Mobility in layer 3 :	60	cm^2 V^-1 s^-1
Mobility in layer 4 :	80	cm^2 V^-1 s^-1
Mobility in the active layer :	73	cm^2 V^-1 s^-1
Optical losses :	30	cm^-1
Radiative constant :	7E-11	cm^3 s^-1
Radiative ratio :	1.7E-19	
Auger coefficient :	8E-29	cm^6 s^-1
Optical efficiency :	0.3	%
Gain coefficient :	2.5E-16	cm^2
Transparency density :	1.5E+18	atoms cm^-3
Reflection coefficient :	0.001	

APPENDIX III (continued)

Calculations :

B(n) cm^3 s^-1	Ja A cm^-2	Io mA	Is mA	Lo cm	2xSy+w µm	ni	D
2.47E-11	9911	25.96	299.7	5.24E-05	8.98	0.075	0.912
2.59E-11	9203	25.01	280.1	5.44E-05	8.94	0.080	
2.72E-11	8496	24.03	260.5	5.66E-05	8.89	0.086	------
2.85E-11	7764	22.98	240.0	5.92E-05	8.84	0.093	1/Rs
3.00E-11	7046	21.89	219.9	6.21E-05	8.79	0.100	ohm^-1
3.14E-11	6346	20.77	200.2	6.55E-05	8.72	0.108	
3.31E-11	5644	19.59	180.3	6.94E-05	8.64	0.117	3E-04
3.48E-11	4949	18.34	160.4	7.41E-05	8.55	0.128	
3.67E-11	4251	17.00	140.3	8.00E-05	8.44	0.141	
3.88E-11	3547	15.53	119.7	8.76E-05	8.29	0.156	
4.11E-11	2892	14.02	100.4	9.70E-05	8.10	0.174	
4.38E-11	2213	12.27	79.9	1.11E-04	7.83	0.199	
4.69E-11	1582	10.37	60.3	1.31E-04	7.44	0.232	
5.10E-11	953	8.05	39.9	1.69E-04	6.70	0.285	
5.67E-11	382	5.09	19.7	2.67E-04	5.22	0.387	

g cm^-1	Gs	Gsm	Psp µW	Po mW	Gmax	Gmin	M %
5.76E+02	3.0E+03	3.8E+02	5.46E+01	2.08E+01	9.87E+02	1.99E+02	66.36
5.51E+02	2.1E+03	2.8E+02	5.42E+01	1.50E+01	5.25E+02	1.69E+02	51.22
5.25E+02	1.4E+03	2.0E+02	5.37E+01	1.06E+01	3.06E+02	1.38E+02	37.98
4.96E+02	9.4E+02	1.4E+02	5.28E+01	7.31E+00	1.84E+02	1.06E+02	26.95
4.66E+02	6.1E+02	9.4E+01	5.17E+01	4.93E+00	1.15E+02	7.88E+01	18.71
4.35E+02	3.8E+02	6.4E+01	5.03E+01	3.28E+00	7.33E+01	5.67E+01	12.79
4.01E+02	2.3E+02	4.3E+01	4.86E+01	2.12E+00	4.65E+01	3.92E+01	8.50
3.65E+02	1.4E+02	2.8E+01	4.65E+01	1.33E+00	2.92E+01	2.62E+01	5.52
3.25E+02	7.6E+01	1.7E+01	4.39E+01	8.04E-01	1.80E+01	1.68E+01	3.47
2.80E+02	3.9E+01	1.0E+01	4.06E+01	4.65E-01	1.07E+01	1.02E+01	2.09
2.33E+02	2.0E+01	6.2E+00	3.70E+01	2.68E-01	6.32E+00	6.17E+00	1.25
1.75E+02	8.4E+00	3.5E+00	3.23E+01	1.45E-01	3.50E+00	3.46E+00	0.70
1.10E+02	3.2E+00	1.9E+00	2.69E+01	7.82E-02	1.91E+00	1.90E+00	0.38
2.50E+01	9.3E-01	9.6E-01	1.99E+01	3.91E-02	9.66E-01	9.62E-01	0.19
-9.50E+01	1.6E-01	4.6E-01	1.08E+01	1.58E-02	4.58E-01	4.57E-01	0.09

APPENDIX III (continued)

Calculated results :

Resistivity of layer 3 :	0.0521 ohms cm
Resistivity of layer 4 :	0.0391 ohms cm
Resistivity of the active layer :	0.1712 ohms cm
Sheet resistivity of the 3 layers :	3824 ohms
Confinement factor :	0.294
Broad area internal quantum efficiency :	10.1 %
Internal quantum eff. at 7046 A cm^-2 :	10.0 %

Carrier Density cm^-3	Spontaneous Coefficient cm^3 s^-1	Drive Current mA	Output Power mW	Modulation Depth %	Actual Power mW	Actual Modulation Depth, %
3.81E+18	2.47E-11	300	20.78	66.36		
3.71E+18	2.59E-11	280	15.00	51.22		
3.60E+18	2.72E-11	260	10.65	37.98		
3.49E+18	2.85E-11	240	7.31	26.95	7.50	
3.37E+18	3.00E-11	220	4.93	18.71	5.00	18.6
3.24E+18	3.14E-11	200	3.28	12.79	3.00	
3.11E+18	3.31E-11	180	2.12	8.50	1.90	
2.96E+18	3.48E-11	160	1.33	5.52	1.23	5.2
2.80E+18	3.67E-11	140	0.80	3.47	0.80	
2.62E+18	3.88E-11	120	0.46	2.09	0.51	
2.43E+18	4.11E-11	100	0.27	1.25	0.31	
2.20E+18	4.38E-11	80	0.14	0.70	0.17	
1.94E+18	4.69E-11	60	0.08	0.38	0.06	
1.60E+18	5.10E-11	40	0.04	0.19	0.00	
1.12E+18	5.67E-11	20	0.02	0.09	0.00	

APPENDIX IV: The spreadsheet study of A1159#M3

Measured values :

Doping level of layer 3 :	2E+18 atoms cm^-3
Doping level of layer 4 :	2E+18 atoms cm^-3
Doping level of the active region :	5E+17 atoms cm^-3
Thickness of layer 3 :	0.07 µm
Thickness of layer 4 :	0.02 µm
Thickness of the active layer :	0.13 µm
Ridge width :	5 µm
Cavity length :	500 µm
Broad area threshold current density :	7000 A cm^-2
Wavelength :	1.27 µm

Assumed values :

Mobility in layer 3 :	60 cm^2 V^-1 s^-1
Mobility in layer 4 :	80 cm^2 V^-1 s^-1
Mobility in the active layer :	73 cm^2 V^-1 s^-1
Optical losses :	30 cm^-1
Radiative constant :	6E-11 cm^3 s^-1
Radiative ratio :	2.05E-19
Auger coefficient :	5E-29 cm^6 s^-1
Optical efficiency :	0.17 %
Gain coefficient :	1.4E-16 cm^2
Transparency density :	1.5E+18 atoms cm^-3
Reflection coefficient :	0.001

APPENDIX IV (continued)

Calculations :

B(n) cm^3 s^-1	Ja A cm^-2	Io mA	Is mA	Lo cm	2xSy+w µm	ni	D
4.16E-12	9910	25.96	299.7	5.24E-05	8.98	0.018	0.912
5.63E-12	9209	25.02	280.3	5.43E-05	8.94	0.025	
7.23E-12	8488	24.02	260.2	5.66E-05	8.89	0.033	------
8.96E-12	7754	22.96	239.8	5.92E-05	8.84	0.041	1/Rs
1.07E-11	7063	21.91	220.4	6.21E-05	8.79	0.051	ohm^-1
1.26E-11	6325	20.74	199.6	6.56E-05	8.72	0.062	
1.46E-11	5639	19.58	180.1	6.94E-05	8.64	0.073	3E-04
1.68E-11	4929	18.31	159.8	7.43E-05	8.55	0.087	
1.92E-11	4245	16.99	140.1	8.00E-05	8.43	0.103	
2.17E-11	3566	15.57	120.3	8.73E-05	8.29	0.123	
2.47E-11	2882	14.00	100.0	9.72E-05	8.10	0.147	
2.80E-11	2222	12.29	80.1	1.11E-04	7.84	0.177	
3.21E-11	1560	10.30	59.6	1.32E-04	7.42	0.220	
3.70E-11	949	8.03	39.8	1.69E-04	6.69	0.284	
4.40E-11	383	5.10	19.8	2.66E-04	5.21	0.404	

g cm^-1	Gs	Gsm	Psp µW	Po mW	Gmax	Gmin	M %
4.26E+02	3.3E+02	5.7E+01	7.41E+00	4.31E-01	6.44E+01	5.12E+01	11.41
4.09E+02	2.6E+02	4.7E+01	9.51E+00	4.53E-01	5.13E+01	4.26E+01	9.31
3.91E+02	2.0E+02	3.7E+01	1.15E+01	4.43E-01	4.04E+01	3.48E+01	7.48
3.71E+02	1.5E+02	3.0E+01	1.33E+01	4.09E-01	3.15E+01	2.80E+01	5.93
3.51E+02	1.1E+02	2.4E+01	1.48E+01	3.64E-01	2.47E+01	2.25E+01	4.71
3.29E+02	8.1E+01	1.8E+01	1.62E+01	3.10E-01	1.88E+01	1.75E+01	3.63
3.07E+02	5.8E+01	1.4E+01	1.72E+01	2.59E-01	1.45E+01	1.37E+01	2.81
2.81E+02	4.0E+01	1.1E+01	1.79E+01	2.08E-01	1.08E+01	1.04E+01	2.12
2.55E+02	2.7E+01	7.9E+00	1.83E+01	1.63E-01	8.05E+00	7.80E+00	1.58
2.25E+02	1.8E+01	5.8E+00	1.82E+01	1.24E-01	5.86E+00	5.73E+00	1.16
1.92E+02	1.1E+01	4.1E+00	1.76E+01	8.98E-02	4.14E+00	4.08E+00	0.82
1.54E+02	6.2E+00	2.8E+00	1.64E+01	6.29E-02	2.86E+00	2.83E+00	0.57
1.08E+02	3.1E+00	1.9E+00	1.43E+01	4.10E-02	1.88E+00	1.86E+00	0.37
5.18E+01	1.4E+00	1.2E+00	1.12E+01	2.44E-02	1.18E+00	1.18E+00	0.24
-2.80E+01	4.3E-01	6.7E-01	6.43E+00	1.08E-02	6.74E-01	6.72E-01	0.13

APPENDIX IV (continued)

Calculated results :

Resistivity of layer 3 :	0.0521 ohms cm
Resistivity of layer 4 :	0.0391 ohms cm
Resistivity of the active layer :	0.1712 ohms cm
Sheet resistivity of the 3 layers :	3824 ohms
Confinement factor :	0.294
Broad area internal quantum efficiency :	10.1 %
Internal quantum eff. at 7063 A cm^-2 :	5.1 %

Carrier Density cm^-3	Spontaneous Coefficient cm^3 s^-1	Drive Current mA	Output Power mW	Modulation Depth %	Actual Power mW
4.54E+18	4.16E-12	300	0.43	11.41	0.43
4.42E+18	5.63E-12	280	0.45	9.31	0.44
4.29E+18	7.23E-12	260	0.44	7.48	0.44
4.15E+18	8.96E-12	240	0.41	5.93	0.44
4.01E+18	1.07E-11	220	0.36	4.71	0.43
3.85E+18	1.26E-11	200	0.31	3.63	0.40
3.69E+18	1.46E-11	180	0.26	2.81	0.39
3.51E+18	1.68E-11	160	0.21	2.12	0.37
3.32E+18	1.92E-11	140	0.16	1.58	0.30
3.11E+18	2.17E-11	120	0.12	1.16	0.24
2.87E+18	2.47E-11	100	0.09	0.82	0.19
2.60E+18	2.80E-11	80	0.06	0.57	0.10
2.27E+18	3.21E-11	60	0.04	0.37	0.02
1.87E+18	3.70E-11	40	0.02	0.24	0.00
1.30E+18	4.40E-11	20	0.01	0.13	0.00

APPENDIX V: The spreadsheet study of OM653#3

Measured values :

Doping level of layer 3 :	8E+17 atoms cm^-3
Doping level of layer 4 :	8E+17 atoms cm^-3
Doping level of the active region :	1E+17 atoms cm^-3
Thickness of layer 3 :	0.05 µm
Thickness of layer 4 :	0.1 µm
Thickness of the active layer :	0.11 µm
Ridge width :	5 µm
Cavity length :	500 µm
Broad area threshold current density :	3751 A cm^-2
Wavelength :	1.28 µm

Assumed values :

Mobility in layer 3 :	65 cm^2 V^-1 s^-1
Mobility in layer 4 :	90 cm^2 V^-1 s^-1
Mobility in the active layer :	80 cm^2 V^-1 s^-1
Optical losses :	30 cm^-1
Radiative constant :	7E-11 cm^3 s^-1
Radiative ratio :	2.1E-19
Auger coefficient :	9E-29 cm^6 s^-1
Optical efficiency :	0.26 %
Gain coefficient :	1.2E-16 cm^2
Transparency density :	1.5E+18 atoms cm^-3
Reflection coefficient :	0.002

APPENDIX V (continued)

Calculations :

B(n) cm^3 s^-1	Ja A cm^-2	Io mA	Is mA	Lo cm	2xSy+w µm	ni	D
2.00E-11	6633	17.17	200.2	5.18E-05	8.99	0.061	0.766
2.21E-11	5901	16.19	179.9	5.49E-05	8.93	0.070	
2.43E-11	5178	15.17	159.8	5.86E-05	8.85	0.080	------
2.66E-11	4474	14.10	140.1	6.30E-05	8.77	0.091	1/Rs
2.93E-11	3762	12.93	119.9	6.87E-05	8.66	0.105	ohm^-1
3.22E-11	3063	11.67	99.9	7.62E-05	8.51	0.122	
3.56E-11	2373	10.27	79.9	8.65E-05	8.31	0.145	2E-04
3.96E-11	1703	8.70	60.0	1.02E-04	8.00	0.175	
4.47E-11	1039	6.79	39.6	1.31E-04	7.44	0.224	
5.16E-11	451	4.48	20.2	1.98E-04	6.12	0.315	

g cm^-1	Gs	Gsm	Psp µW	Po mW	Gmax	Gmin	M %
2.28E+02	9.4E+00	3.8E+00	2.57E+01	1.22E-01	3.81E+00	3.70E+00	1.50
2.11E+02	7.8E+00	3.3E+00	2.60E+01	1.12E-01	3.35E+00	3.27E+00	1.32
1.93E+02	6.4E+00	2.9E+00	2.61E+01	1.02E-01	2.93E+00	2.86E+00	1.16
1.74E+02	5.1E+00	2.5E+00	2.57E+01	9.06E-02	2.55E+00	2.50E+00	1.01
1.52E+02	4.0E+00	2.2E+00	2.49E+01	7.89E-02	2.18E+00	2.15E+00	0.87
1.28E+02	3.1E+00	1.8E+00	2.36E+01	6.70E-02	1.85E+00	1.82E+00	0.74
1.01E+02	2.2E+00	1.5E+00	2.16E+01	5.48E-02	1.54E+00	1.52E+00	0.61
6.84E+01	1.5E+00	1.3E+00	1.88E+01	4.24E-02	1.26E+00	1.25E+00	0.50
2.64E+01	9.6E-01	9.8E-01	1.47E+01	2.91E-02	9.84E-01	9.76E-01	0.39
-3.00E+01	5.1E-01	7.3E-01	8.95E+00	1.54E-02	7.28E-01	7.23E-01	0.29

APPENDIX V (continued)

Calculated results :

Resistivity of layer 3 :	0.1202 ohms cm
Resistivity of layer 4 :	0.0868 ohms cm
Resistivity of the active layer :	0.7813 ohms cm
Sheet resistivity of the 3 layers :	5852 ohms
Confinement factor :	0.227
Broad area internal quantum efficiency :	18.1 %
Internal quantum eff. at 3762 A cm^-2 :	10.5 %

Carrier Density cm^-3	Spontaneous Coefficient cm^3 s^-1	Drive Current mA	Output Power mW	Modulation Depth %	Actual Power mW
3.40E+18	2.00E-11	200	0.122	1.50	0.120
3.26E+18	2.21E-11	180	0.112	1.32	0.110
3.11E+18	2.43E-11	160	0.102	1.16	0.100
2.95E+18	2.66E-11	140	0.091	1.01	0.090
2.77E+18	2.93E-11	120	0.079	0.87	0.080
2.57E+18	3.22E-11	100	0.067	0.74	0.070
2.34E+18	3.56E-11	80	0.055	0.61	0.055
2.07E+18	3.96E-11	60	0.042	0.50	0.040
1.72E+18	4.47E-11	40	0.029	0.39	0.030
1.25E+18	5.16E-11	20	0.015	0.29	0.015

APPENDIX VI: The spreadsheet study of OM653#9

Measured values :

Doping level of layer 3 :	8E+17	atoms cm^-3
Doping level of layer 4 :	8E+17	atoms cm^-3
Doping level of the active region :	1E+17	atoms cm^-3
Thickness of layer 3 :	0.05	µm
Thickness of layer 4 :	0.1	µm
Thickness of the active layer :	0.11	µm
Ridge width :	5	µm
Cavity length :	500	µm
Broad area threshold current density :	3751	A cm^-2
Wavelength :	1.28	µm

Assumed values :

Mobility in layer 3 :	65	cm^2 V^-1 s^-1
Mobility in layer 4 :	90	cm^2 V^-1 s^-1
Mobility in the active layer :	80	cm^2 V^-1 s^-1
Optical losses :	30	cm^-1
Radiative constant :	7E-11	cm^3 s^-1
Radiative ratio :	1.7E-19	
Auger coefficient :	7E-29	cm^6 s^-1
Optical efficiency :	0.35	%
Gain coefficient :	1.2E-16	cm^2
Transparency density :	1.5E+18	atoms cm^-3
Reflection coefficient :	0.002	

APPENDIX VI (continued)

Calculations :

B(n) cm^3 s^-1	Ja A cm^-2	Io mA	Is mA	Lo cm	2xSy+w µm	ni	D
2.66E-11	6614	17.14	199.6	5.18E-05	8.99	0.094	0.766
2.84E-11	5893	16.18	179.7	5.49E-05	8.93	0.104	
3.03E-11	5184	15.18	160.0	5.85E-05	8.86	0.115	------
3.24E-11	4457	14.07	139.6	6.31E-05	8.77	0.128	1/Rs
3.47E-11	3766	12.93	120.0	6.87E-05	8.66	0.143	ohm^-1
3.73E-11	3058	11.66	99.8	7.62E-05	8.51	0.162	
4.01E-11	2393	10.31	80.5	8.62E-05	8.32	0.186	2E-04
4.37E-11	1705	8.70	60.0	1.02E-04	8.00	0.220	
4.81E-11	1054	6.84	40.0	1.30E-04	7.46	0.272	
5.42E-11	458	4.51	20.5	1.97E-04	6.15	0.368	

g cm^-1	Gs	Gsm	Psp µW	Po mW	Gmax	Gmin	M %
2.58E+02	1.3E+01	4.7E+00	5.29E+01	3.03E-01	4.83E+00	4.65E+00	1.90
2.40E+02	1.1E+01	4.1E+00	5.19E+01	2.66E-01	4.19E+00	4.05E+00	1.65
2.21E+02	8.7E+00	3.6E+00	5.04E+01	2.30E-01	3.61E+00	3.51E+00	1.42
1.99E+02	6.8E+00	3.0E+00	4.83E+01	1.95E-01	3.06E+00	2.99E+00	1.21
1.76E+02	5.3E+00	2.6E+00	4.57E+01	1.63E-01	2.59E+00	2.54E+00	1.03
1.50E+02	3.9E+00	2.1E+00	4.21E+01	1.32E-01	2.15E+00	2.11E+00	0.85
1.21E+02	2.8E+00	1.8E+00	3.78E+01	1.04E-01	1.76E+00	1.74E+00	0.70
8.52E+01	1.9E+00	1.4E+00	3.19E+01	7.62E-02	1.40E+00	1.38E+00	0.56
4.08E+01	1.1E+00	1.1E+00	2.43E+01	5.02E-02	1.07E+00	1.06E+00	0.43
-2.04E+01	5.6E-01	7.6E-01	1.43E+01	2.52E-02	7.64E-01	7.60E-01	0.30

APPENDIX VI (continued)

Calculated results :

Resistivity of layer 3 :	0.1202 ohms cm
Resistivity of layer 4 :	0.0868 ohms cm
Resistivity of the active layer :	0.7813 ohms cm
Sheet resistivity of the 3 layers :	5852 ohms
Confinement factor :	0.227
Broad area internal quantum efficiency :	18.1 %
Internal quantum eff. at 3766 A cm^-2 :	14.3 %

Carrier Density cm^-3	Spontaneous Coefficient cm^3 s^-1	Drive Current mA	Output Power mW	Modulation Depth %	Actual Power mW
3.65E+18	2.66E-11	200	0.303	1.90	0.300
3.50E+18	2.84E-11	180	0.266	1.65	0.270
3.34E+18	3.03E-11	160	0.230	1.42	0.230
3.16E+18	3.24E-11	140	0.195	1.21	0.200
2.97E+18	3.47E-11	120	0.163	1.03	0.170
2.75E+18	3.73E-11	100	0.132	0.85	0.140
2.51E+18	4.01E-11	80	0.104	0.70	0.110
2.21E+18	4.37E-11	60	0.076	0.56	0.080
1.84E+18	4.81E-11	40	0.050	0.43	0.055
1.33E+18	5.42E-11	20	0.025	0.30	0.030

APPENDIX VII: The spreadsheet study of the best structure at 150 mA

Measured values :

Doping level of layer 3 :	8E+17 atoms cm^-3
Doping level of layer 4 :	8E+17 atoms cm^-3
Doping level of the active region :	1E+17 atoms cm^-3
Thickness of layer 3 :	0.05 µm
Thickness of layer 4 :	0.05 µm
Thickness of the active layer :	0.22 µm
Ridge width :	5 µm
Wavelength :	1.3 µm

Assumed values :

Mobility in layer 3 :	60 cm^2 V^-1 s^-1
Mobility in layer 4 :	80 cm^2 V^-1 s^-1
Mobility in the active layer :	70 cm^2 V^-1 s^-1
Optical losses :	30 cm^-1
Radiative constant :	7E-11 cm^3 s^-1
Radiative ratio :	1.7E-19
Auger coefficient :	7E-29 cm^6 s^-1
Optical efficiency :	0.4 %
Gain coefficient :	2.5E-16 cm^2
Transparency density :	1.5E+18 atoms cm^-3
Reflection coefficient :	0.0006

APPENDIX VII (continued)

Calculations :

B(n) cm^3 s^-1	Ja A cm^-2	Io mA	Is mA	Lo cm	2xSy+w µm	ni	D
2.63E-11	13428	7.99	150.3	2.97E-05	9.42	0.093	1.508
3.28E-11	8685	9.64	149.6	3.70E-05	9.28	0.130	
3.67E-11	6390	11.02	149.8	4.31E-05	9.16	0.158	------
3.96E-11	5020	12.21	149.9	4.87E-05	9.05	0.181	1/Rs
4.17E-11	4130	13.29	150.5	5.36E-05	8.95	0.201	ohm^-1
4.35E-11	3473	14.22	150.0	5.85E-05	8.86	0.218	
4.50E-11	2999	15.10	150.2	6.29E-05	8.77	0.234	1E-04
4.62E-11	2622	15.88	149.7	6.73E-05	8.68	0.248	
4.72E-11	2340	16.67	150.3	7.13E-05	8.61	0.260	
4.82E-11	2093	17.35	149.8	7.53E-05	8.53	0.273	
4.89E-11	1906	18.06	150.5	7.90E-05	8.46	0.283	
4.97E-11	1730	18.64	149.7	8.29E-05	8.38	0.294	
5.04E-11	1590	19.24	149.7	8.65E-05	8.31	0.304	
5.10E-11	1468	19.81	149.8	8.99E-05	8.24	0.313	
5.15E-11	1365	20.37	149.9	9.33E-05	8.18	0.321	

g cm^-1	Gs	Gsm	Psp µW	Po mW	Gmax	Gmin	M %
5.43E+02	2.3E+02	4.3E+01	4.77E+01	2.08E+00	4.49E+01	4.05E+01	5.11
4.08E+02	4.1E+02	6.8E+01	6.47E+01	4.50E+00	7.44E+01	6.32E+01	8.20
3.24E+02	5.2E+02	8.3E+01	7.72E+01	6.47E+00	9.16E+01	7.51E+01	9.91
2.64E+02	5.0E+02	8.0E+01	8.69E+01	7.08E+00	8.88E+01	7.32E+01	9.63
2.19E+02	4.1E+02	6.8E+01	9.50E+01	6.60E+00	7.44E+01	6.32E+01	8.20
1.81E+02	2.8E+02	4.9E+01	1.01E+02	5.11E+00	5.25E+01	4.66E+01	5.92
1.51E+02	1.7E+02	3.4E+01	1.07E+02	3.70E+00	3.50E+01	3.22E+01	4.03
1.25E+02	9.4E+01	2.1E+01	1.12E+02	2.41E+00	2.11E+01	2.01E+01	2.47
1.04E+02	5.1E+01	1.3E+01	1.16E+02	1.59E+00	1.28E+01	1.24E+01	1.52
8.38E+01	2.3E+01	7.1E+00	1.20E+02	9.67E-01	7.13E+00	7.01E+00	0.85
6.75E+01	1.1E+01	4.2E+00	1.24E+02	6.38E-01	4.18E+00	4.14E+00	0.50
5.13E+01	4.3E+00	2.3E+00	1.26E+02	4.14E-01	2.28E+00	2.27E+00	0.27
3.75E+01	1.7E+00	1.3E+00	1.29E+02	3.02E-01	1.34E+00	1.34E+00	0.16
2.50E+01	6.7E-01	8.2E-01	1.32E+02	2.40E-01	8.25E-01	8.24E-01	0.10
1.38E+01	2.5E-01	5.4E-01	1.34E+02	2.07E-01	5.42E-01	5.41E-01	0.07

APPENDIX VII (continued)

Calculated results :

Resistivity of layer 3 :	0.1302	ohms cm
Resistivity of layer 4 :	0.0977	ohms cm
Resistivity of the active layer :	0.8929	ohms cm
Sheet resistivity of the 3 layers :	8754	ohms
Confinement factor :	0.532	
Internal quantum eff. at 4130 a cm^-2 :	16.3	%

Cavity Length µm	Carrier Density cm^-3	Spontaneous Coefficient cm^3 s^-1	Drive Current mA	Output Power mW	Modulation Depth %
200	3.67E+18	2.63E-11	150	2.08	5.11
300	3.13E+18	3.28E-11	150	4.50	8.20
400	2.80E+18	3.67E-11	150	6.47	9.91
500	2.56E+18	3.96E-11	150	7.08	9.63
600	2.38E+18	4.17E-11	150	6.60	8.20
700	2.23E+18	4.35E-11	150	5.11	5.92
800	2.11E+18	4.50E-11	150	3.70	4.03
900	2.00E+18	4.62E-11	150	2.41	2.47
1000	1.92E+18	4.72E-11	150	1.59	1.52
1100	1.84E+18	4.82E-11	150	0.97	0.85
1200	1.77E+18	4.89E-11	150	0.64	0.50
1300	1.71E+18	4.97E-11	150	0.41	0.27
1400	1.65E+18	5.04E-11	150	0.30	0.16
1500	1.60E+18	5.10E-11	150	0.24	0.10
1600	1.56E+18	5.15E-11	150	0.21	0.07

APPENDIX VIII: The spreadsheet study of the best structure at 160 mA

Measured values :

Doping level of layer 3 :	8E+17	atoms cm^-3
Doping level of layer 4 :	8E+17	atoms cm^-3
Doping level of the active region :	1E+17	atoms cm^-3
Thickness of layer 3 :	0.05	µm
Thickness of layer 4 :	0.05	µm
Thickness of the active layer :	0.22	µm
Ridge width :	5	µm
Wavelength :	1.3	µm

Assumed values :

Mobility in layer 3 :	60	cm^2 V^-1 s^-1
Mobility in layer 4 :	80	cm^2 V^-1 s^-1
Mobility in the active layer :	70	cm^2 V^-1 s^-1
Optical losses :	30	cm^-1
Radiative constant :	7E-11	cm^3 s^-1
Radiative ratio :	1.7E-19	
Auger coefficient :	7E-29	cm^6 s^-1
Optical efficiency :	0.4	%
Gain coefficient :	2.5E-16	cm^2
Transparency density :	1.5E+18	atoms cm^-3
Reflection coefficient :	0.0004	

APPENDIX VII (continued)

Calculations :

B(n) cm^3 s^-1	Ja A cm^-2	Io mA	Is mA	Lo cm	2xSy+w µm	ni	D
2.53E-11	14355	8.26	160.1	2.88E-05	9.44	0.088	1.508
3.17E-11	9343	10.00	160.1	3.57E-05	9.30	0.124	
3.58E-11	6864	11.42	160.1	4.16E-05	9.19	0.151	------
3.88E-11	5397	12.66	160.2	4.69E-05	9.08	0.174	1/Rs
4.10E-11	4414	13.74	159.9	5.19E-05	8.99	0.194	ohm^-1
4.28E-11	3726	14.73	159.9	5.65E-05	8.90	0.211	
4.43E-11	3211	15.62	159.7	6.08E-05	8.81	0.227	1E-04
4.55E-11	2815	16.46	159.6	6.50E-05	8.73	0.240	
4.66E-11	2503	17.25	159.6	6.89E-05	8.65	0.253	
4.75E-11	2261	18.03	160.4	7.25E-05	8.58	0.264	
4.83E-11	2049	18.72	160.4	7.61E-05	8.51	0.275	
4.91E-11	1864	19.35	159.9	7.98E-05	8.44	0.286	
4.98E-11	1717	20.00	160.2	8.32E-05	8.37	0.295	
5.04E-11	1590	20.61	160.4	8.65E-05	8.31	0.304	
5.10E-11	1468	21.13	159.7	8.99E-05	8.24	0.313	

g cm^-1	Gs	Gsm	Psp µW	Po mW	Gmax	Gmin	M %
5.65E+02	3.0E+02	5.2E+01	4.80E+01	2.54E+00	5.41E+01	4.98E+01	4.15
4.29E+02	5.8E+02	9.1E+01	6.62E+01	6.09E+00	9.80E+01	8.48E+01	7.27
3.43E+02	7.7E+02	1.2E+02	7.94E+01	9.29E+00	1.28E+02	1.06E+02	9.26
2.81E+02	8.0E+02	1.2E+02	8.98E+01	1.08E+01	1.32E+02	1.09E+02	9.53
2.34E+02	6.7E+02	1.0E+02	9.81E+01	1.02E+01	1.11E+02	9.45E+01	8.18
1.96E+02	4.9E+02	7.9E+01	1.05E+02	8.38E+00	8.39E+01	7.40E+01	6.29
1.65E+02	3.1E+02	5.4E+01	1.11E+02	6.14E+00	5.67E+01	5.20E+01	4.34
1.39E+02	1.8E+02	3.5E+01	1.16E+02	4.17E+00	3.58E+01	3.39E+01	2.79
1.16E+02	9.8E+01	2.1E+01	1.21E+02	2.69E+00	2.16E+01	2.09E+01	1.70
9.75E+01	5.2E+01	1.3E+01	1.26E+02	1.74E+00	1.30E+01	1.28E+01	1.03
8.00E+01	2.4E+01	7.3E+00	1.29E+02	1.07E+00	7.35E+00	7.27E+00	0.58
6.38E+01	1.0E+01	4.0E+00	1.32E+02	6.60E-01	4.01E+00	3.98E+00	0.32
5.00E+01	4.4E+00	2.3E+00	1.35E+02	4.48E-01	2.31E+00	2.30E+00	0.18
3.75E+01	1.8E+00	1.4E+00	1.38E+02	3.28E-01	1.37E+00	1.37E+00	0.11
2.50E+01	6.5E-01	8.1E-01	1.40E+02	2.55E-01	8.15E-01	8.14E-01	0.07

APPENDIX VII (continued)

Calculated results :

Resistivity of layer 3 :	0.1302 ohms cm
Resistivity of layer 4 :	0.0977 ohms cm
Resistivity of the active layer :	0.8929 ohms cm
Sheet resistivity of the 3 layers :	8754 ohms
Confinement factor :	0.532
Internal quantum eff. at 3726 a cm^-2 :	21.1 %

Cavity Length µm	Carrier Density cm^-3	Spontaneous Coefficient cm^3 s^-1	Drive Current mA	Output Power mW	Modulation Depth %
200	3.76E+18	2.53E-11	160	2.54	4.15
300	3.22E+18	3.17E-11	160	6.09	7.27
400	2.87E+18	3.58E-11	160	9.29	9.26
500	2.63E+18	3.88E-11	160	10.81	9.53
600	2.44E+18	4.10E-11	160	10.15	8.18
700	2.29E+18	4.28E-11	160	8.38	6.29
800	2.16E+18	4.43E-11	160	6.14	4.34
900	2.06E+18	4.55E-11	160	4.17	2.79
1000	1.97E+18	4.66E-11	160	2.69	1.70
1100	1.89E+18	4.75E-11	160	1.74	1.03
1200	1.82E+18	4.83E-11	160	1.07	0.58
1300	1.76E+18	4.91E-11	160	0.66	0.32
1400	1.70E+18	4.98E-11	160	0.45	0.18
1500	1.65E+18	5.04E-11	160	0.33	0.11
1600	1.60E+18	5.10E-11	160	0.25	0.07

APPENDIX IX: The photograph of the 50 μm fiber

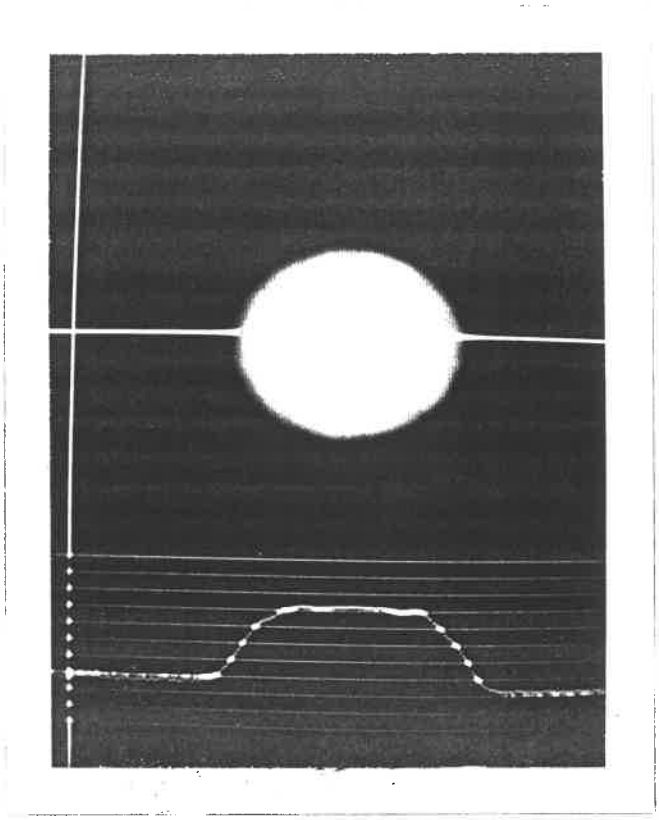

These are the power intensity plots made by a special video analyser attachment to a CCD camera. The photograph is of the monitor, taken with a Polaroid camera. The 50 μm core fiber measures 3.6 cm at the zero intensity points.

APPENDIX X: The costing study of the best cost option

Material Costs			Cost, $				
Seq.	Description	Quantity	Each piece	1	10	100	1000	10000
100	Grown Wafer (1 in 2 good)							
102	Indium Phosphide	0.003	443.04	886.08	1772.16	3544.32	2658.24	26582.40
102	Zinc Metal	0.003	2.0448	4.09	8.18	16.36	12.27	122.69
102	Gallium Metal	0.003	2.0448	4.09	8.18	16.36	12.27	122.69
102	Indium Metal	0.003	21.06144	42.12	84.25	168.49	126.37	1263.69
200	Evaluated Wafer							
210	Gold	0.003	0.00565	0.01	0.02	0.05	0.03	0.34
224	Preform SnPb	0.003	0.53748	1.07	2.15	4.30	3.22	32.25
202	Silane	0.003	0.00242	0.00	0.01	0.02	0.01	0.15
208	Wire, AuZn	0.003	0.13884	0.28	0.56	1.11	0.83	8.33
210	Platinum	0.003	6.77756	13.56	27.11	54.22	40.67	406.65
210	Titanium	0.003	0.08198	0.16	0.33	0.66	0.49	4.92
302	Scandium Oxide	0.003	1.9771	3.95	7.91	15.82	11.86	118.63
213	Nickel	0.003	0.0125	0.03	0.05	0.10	0.08	0.75
213	Germanium	0.003	0.00516	0.01	0.02	0.04	0.03	0.31
224	Header, 10/32	0.003	14.93	29.86	59.72	119.44	89.58	895.80
300	Coated Chips							
302	Scandium Oxide	1.7	0.00085	0.00	0.01	0.14	1.45	14.45
400	Assembled Submount							
401	Preform, SnPb	1.5	0.51073	0.77	7.66	76.61	766.10	7660.95
401	Preform, SnPb	1.5	0.34409	0.52	5.16	51.61	516.14	5161.35
401	Submount, Wired	1.5	61.72	92.58	925.80	8332.20	74064.00	648060.00
500	DIL With Cooler							
507	Solder, SnPb	1.3	0.108	0.14	1.40	14.04	140.40	1404.00
502	TE Cooler	1.4	43.717	61.20	612.04	5508.34	48963.04	428426.60
505	Insulating Tube	1.4	0.68	0.95	9.52	85.68	761.60	5712.00
501	DIL Package	1.4	23.18	32.45	324.52	2920.68	25961.60	194712.00
600	Fiber Assembly							
601	Heat Shrink,.027"	1.5	0.0031	0.00	0.05	0.47	4.65	46.50
601	Solder Ball, AuSn	1.5	0.23377	0.35	3.51	35.07	350.66	3506.55
601	Fiber, 9µm, Lens	1.5	54.58331	81.87	818.75	7368.75	65499.97	491249.79
601	Tube, Plated	1.5	2.67567	4.01	40.14	401.35	4013.51	40135.05
700	Untested SLD							
706	Gold wire,.002"	1.3	0.0166	0.02	0.22	2.16	21.58	215.80
703	Epoxy, H70E	1.3	0.00032	0.00	0.00	0.04	0.42	4.16
728	Heat Shrink,.125"	1.11	0.02475	0.03	0.27	2.75	27.47	274.73
726	Black Ink	1.11	0.07849	0.09	0.87	8.71	87.12	871.24
707	Preform, InSn	1.3	3.13745	4.08	40.79	407.87	4078.69	40786.85

APPENDIX X (continued)

Material Costs				Cost, $				
Seq.	Description	Quantity	Each piece	1	10	100	1000	10000
727	Epoxy, Torrseal	1.15	0.00045	0.00	0.01	0.05	0.52	5.18
723	Cleaned Cover	1.15	1.26571	1.46	14.56	145.56	1455.57	14555.66
710	Sleeve Clamp	1.2	5.5575	6.67	66.69	600.21	5335.20	40014.00
711	Solder, InSn	1.2	0.21475	0.26	2.58	25.77	257.70	2577.00
701	Thermistor	1.3	8.42843	10.96	109.57	986.13	8765.57	65741.75
710	Screws, 0-80	1.2	1.14192	1.37	13.70	137.03	1370.30	13703.04
710	Fiber Support	1.2	10.13571	12.16	121.63	1094.66	9730.28	85139.96
701	Ceramic, S/off	1.3	17.72114	23.04	230.37	2073.37	18429.99	138224.89
717	Detector Assy	1.15	15.60663	17.95	179.48	1615.29	14358.10	125633.37
800	Tested SLD							
808	Label, ESD	1	0.092	0.09	0.92	9.20	92.00	920
808	Label, Contents	1	0.12	0.12	1.20	12.00	120.00	1200
808	Label, Warning	1	0.19	0.19	1.90	19.00	190.00	1900
808	Label, Danger	1	0.19	0.19	1.90	19.00	190.00	1900
808	Label, DIL	1	0.137	0.14	1.37	13.70	137.00	1370
808	Foam, .5"	1	0.35	0.35	3.50	35.00	350.00	3500
808	Foam, .25"	1	0.6	0.60	6.00	60.00	600.00	6000
808	Box	1	1.05	1.05	10.50	105.00	1050.00	10500
	Total, $			1341.98	5537.22	36208.70	291646.55	2420686.46

Routing Costs				Cost, $				
Seq.	Description	Factor	Hrs/piece	1	10	100	1000	10000
100	Grown Wafer (1 in 2 good)							
101	Prepare Substrate		0.3036	7.98	7.98	7.98	23.94	239.36
102	Grow Wafer		3.082	80.99	80.99	80.99	242.98	2429.85
103	Inspect Wafer		0.1857	4.88	4.88	4.88	14.64	146.41
200	Evaluated Wafer							
201	Prepare Wafer		0.01	0.26	0.26	0.26	0.79	7.88
202	Deposit SiO2		0.1	2.63	2.63	2.63	7.88	78.84
203	Coat Photoresist		0.01	0.26	0.26	0.26	0.79	7.88
204	Align Mask		0.01	0.26	0.26	0.26	0.79	7.88
205	Develop Photoresist		0.6	15.77	15.77	15.77	47.30	473.04
206	Open Contact		0.125	3.29	3.29	3.29	9.86	98.55
203A	Coat Photoresist		0.01	0.26	0.26	0.26	0.79	7.88
204A	Align Mask		0.01	0.26	0.26	0.26	0.79	7.88
205A	Develop Photoresist		0.6	15.77	15.77	15.77	47.30	473.04
206A	Open Contact		0.125	3.29	3.29	3.29	9.86	98.55

APPENDIX X (continued)

Routing Costs				Cost, $				
Seq.	Description	Factor	Hrs/piece	1	10	100	1000	10000
207	Clean, J100		0.05	1.31	1.31	1.31	3.94	39.42
208	Deposit AuZn		0.1	2.63	2.63	2.63	7.88	78.84
209	Strip AuZn		0.02	0.53	0.53	0.53	1.58	15.77
210	P Metal Evap.		0.4	10.51	10.51	10.51	31.54	315.36
211	Mount Wafer		0.01	0.26	0.26	0.26	0.79	7.88
212	Clean J100		0.05	1.31	1.31	1.31	3.94	39.42
213	N Metal Evap.		0.4	10.51	10.51	10.51	31.54	315.36
214	Fast Alloy		0.05	1.31	1.31	1.31	3.94	39.42
215	N Metal Evap.		0.2	5.26	5.26	5.26	15.77	157.68
216	Evaluation Cleave		0.2	5.26	5.26	5.26	15.77	157.68
217	Load Coater		0.2	5.26	5.26	5.26	15.77	157.68
218	Coat Facet		0.2	5.26	5.26	5.26	15.77	157.68
219	Reload Coater		0.125	3.29	3.29	3.29	9.86	98.55
220	Coat Facet		0.2	5.26	5.26	5.26	15.77	157.68
221	Unload Coater		0.1	2.63	2.63	2.63	7.88	78.84
222	Separate Scribe		0.5	13.14	13.14	13.14	39.42	394.20
223	Visual Inspection		0.25	6.57	6.57	6.57	19.71	197.10
224	Manual Bond		0.5	13.14	13.14	13.14	39.42	394.20
225	Clean Assy.		0.1	2.63	2.63	2.63	7.88	78.84
226	Inspect Assy.		0.1	2.63	2.63	2.63	7.88	78.84
227	Test Power		0.25	6.57	6.57	6.57	19.71	197.10
228	Test Vf		0.05	1.31	1.31	1.31	3.94	39.42
229	Test Wavelength		0.5	13.14	13.14	13.14	39.42	394.20
230	Burn in		0.01	0.26	0.26	0.26	0.79	7.88
231	Test Power		0.25	6.57	6.57	6.57	19.71	197.10
232	Interpret Data		0.1	2.63	2.63	2.63	7.88	78.84
300	Coated Chips							
301	Cleave Bars	1.7	0.00062	0.01	0.14	1.38	13.85	138.50
302	Load Coater	1.7	0.00031	0.01	0.07	0.69	6.92	69.25
303	Coat Facet	1.7	0.00031	0.01	0.07	0.69	6.92	69.25
304	Reload Coater	1.7	0.00031	0.01	0.07	0.69	6.92	69.25
305	Coat Facet	1.7	0.00031	0.01	0.07	0.69	6.92	69.25
306	Unload Coater	1.7	0.00016	0.00	0.04	0.36	3.57	35.74
307	Scribe Chips	1.7	0.00156	0.03	0.35	3.48	34.85	348.47
308	Inspect Chips	1.7	0.00078	0.02	0.17	1.74	17.42	174.24
400	Assembled Submount							
401	Manual Bond	1.5	0.05	0.99	9.86	98.55	985.50	9855.00
402	Clean Assy.	1.5	0.01	0.20	1.97	19.71	197.10	1971.00
403	Inspect Assy.	1.5	0.01	0.20	1.97	19.71	197.10	1971.00
404	Test Power	1.4	0.05	0.92	9.20	91.98	919.80	9198.00

APPENDIX X (continued)

Routing Costs				Cost, $				
Seq.	Description	Factor	Hrs/piece	1	10	100	1000	10000
405	Burn in	1.4	0.005	0.09	0.92	9.20	91.98	919.80
406	Test Power	1.4	0.05	0.92	9.20	91.98	919.80	9198.00
407	Inspect Assy.	1.3	0.017	0.29	2.90	29.04	290.39	2903.94
500	DIL with Cooler							
501	Clean Package	1.4	0.017	0.31	3.13	31.27	312.73	3127.32
502	Clean Coolers	1.4	0.034	0.63	6.25	62.55	625.46	6254.64
503	Solder Cooler	1.4	0.1	1.84	18.40	183.96	1839.60	18396.00
504	Clean Assy.	1.4	0.017	0.31	3.13	31.27	312.73	3127.32
505	Fit Tubes	1.4	0.017	0.31	3.13	31.27	312.73	3127.32
506	Test Cooler	1.4	0.017	0.31	3.13	31.27	312.73	3127.32
507	Solder Wires	1.3	0.017	0.29	2.90	29.04	290.39	2903.94
600	Fiber Assembly							
601	Solder Tube	1.5	0.043	0.85	8.48	84.75	847.53	8475.30
602	Shrink Tubing	1.3	0.043	0.73	7.35	73.45	734.53	7345.26
603	Label Lot	1.3	0.006	0.10	1.02	10.25	102.49	1024.92
700	Untested SLD							
701	Solder Thermistor	1.3	0.034	0.58	5.81	58.08	580.79	5807.88
702	Clean Assy.	1.3	0.0085	0.15	1.45	14.52	145.20	1451.97
703	Epoxy Submount	1.3	0.0085	0.15	1.45	14.52	145.20	1451.97
704	Bake	1.3	0.0001	0.00	0.02	0.17	1.71	17.08
705	Remove Spacers	1.3	0.0085	0.15	1.45	14.52	145.20	1451.97
706	Wire Bond	1.3	0.01	0.17	1.71	17.08	170.82	1708.20
707	Solder Submount	1.3	0.05	0.85	8.54	85.41	854.10	8541.00
708	Wire Bond	1.3	0.01	0.17	1.71	17.08	170.82	1708.20
709	Optimize Align.	1.3	0.067	1.14	11.44	114.45	1144.49	11444.94
710	Clamp Fiber	1.2	0.067	1.06	10.56	105.65	1056.46	10564.56
711	Solder Feedthroug	1.2	0.067	1.06	10.56	105.65	1056.46	10564.56
712	Recover Power	1.2	0.083	1.31	13.09	130.87	1308.74	13087.44
713	Bake	1.2	0.0001	0.00	0.02	0.16	1.58	15.77
714	Recover Power	1.2	0.083	1.31	13.09	130.87	1308.74	13087.44
715	Bake	1.2	0.0001	0.00	0.02	0.16	1.58	15.77
716	Test Power	1.2	0.083	1.31	13.09	130.87	1308.74	13087.44
717	Epoxy Photodiode	1.15	0.017	0.26	2.57	25.69	256.89	2568.87
718	Bake	1.15	0.0001	0.00	0.02	0.15	1.51	15.11
719	Wire Bond	1.15	0.01	0.15	1.51	15.11	151.11	1511.10
720	Test Photodiode	1.15	0.01	0.15	1.51	15.11	151.11	1511.10
721	Fine Leak Test	1.15	0.0417	0.63	6.30	63.01	630.13	6301.29
722	Inspect	1.15	0.018	0.27	2.72	27.20	272.00	2719.98
723	Seam Seal	1.15	0.01	0.15	1.51	15.11	151.11	1511.10

APPENDIX X (continued)

Routing Costs				Cost, $				
Seq.	Description	Factor	Hrs/piece	1	10	100	1000	10000
724	Fine Leak Test	1.12	0.0417	0.61	6.14	61.37	613.69	6136.91
725	Gross Leak Test	1.11	0.017	0.25	2.48	24.80	247.95	2479.52
726	Mark Devices	1.11	0.034	0.50	4.96	49.59	495.90	4959.04
727	Apply Sealant	1.11	0.0085	0.12	1.24	12.40	123.98	1239.76
728	Add Heatshrink	1.11	0.0085	0.12	1.24	12.40	123.98	1239.76
800	Tested SLD							
801	Test Power	1.11	0.091	1.33	13.27	132.73	1327.27	13272.71
802	Thermal Shock	1.1	0.001	0.01	0.14	1.45	14.45	144.54
803	Burn in	1.1	0.01	0.14	1.45	14.45	144.54	1445.40
804	Test power	1.1	0.091	1.32	13.15	131.53	1315.31	13153.14
805	Test power, Hot	1.07	0.091	1.28	12.79	127.94	1279.44	12794.42
806	Test Wavelength	1.05	0.091	1.26	12.56	125.55	1255.53	12555.27
807	Inspection	1	0.0078	0.10	1.02	10.25	102.49	1024.92
808	Pack Devices	1	0.034	0.45	4.47	44.68	446.76	4467.60
	Total,$			295.96	574.02	3354.64	31690.98	316909.77

Summary	Cost, $				
Quantity / annum	1	10	100	1000	10000
Material Cost	1341.98	5537.22	36208.70	291646.55	2420686.46
Handling Cost	150.97	622.94	4073.48	32810.24	272327.23
Direct Labor Cost	295.96	574.02	3354.64	31690.98	316909.77
Fixed Overhead	1189.76	2307.57	13485.66	127397.72	1273977.28
Cost of Sales	2978.67	9041.74	57122.48	483545.49	4283900.74
Unit Cost	2978.67	904.17	571.22	483.55	428.39

APPENDIX XI: The costing study for the worse cost option

Material Costs			Cost, $				
Seq.	Description	Quantity	Each piece	1	10	100	1000	10000
100	Grown Wafer (1 in 10 good)							
102	Indium Phosphide	0.003	443.04	4430.40	4430.40	4430.40	13291.20	132912.00
102	Zinc Metal	0.003	2.0448	20.45	20.45	20.45	61.34	613.44
102	Gallium Metal	0.003	2.0448	20.45	20.45	20.45	61.34	613.44
102	Indium Metal	0.003	21.06144	210.61	210.61	210.61	631.84	6318.43
200	Evaluated Wafer							
210	Gold	0.003	0.00565	0.06	0.06	0.06	0.17	1.70
224	Preform SnPb	0.003	0.53748	5.37	5.37	5.37	16.12	161.24
202	Silane	0.003	0.00242	0.02	0.02	0.02	0.07	0.73
208	Wire, AuZn	0.003	0.13884	1.39	1.39	1.39	4.17	41.65
210	Platinum	0.003	6.77756	67.78	67.78	67.78	203.33	2033.27
210	Titanium	0.003	0.08198	0.82	0.82	0.82	2.46	24.59
302	Scandium Oxide	0.003	1.9771	19.77	19.77	19.77	59.31	593.13
213	Nickel	0.003	0.0125	0.13	0.13	0.13	0.38	3.75
213	Germanium	0.003	0.00516	0.05	0.05	0.05	0.15	1.55
224	Header, 10/32	0.003	14.93	149.30	149.30	149.30	447.90	4479.00
300	Coated Chips							
302	Scandium Oxide	2.5	0.00085	0.00	0.02	0.21	2.13	21.25
400	Assembled Submount							
401	Preform, SnPb	2	0.51073	1.02	10.21	102.15	1021.46	10214.60
401	Preform, SnPb	2	0.34409	0.69	6.88	68.82	688.18	6881.80
401	Submount, Wired	2	61.72	123.44	1234.40	11109.60	98752.00	864080.00
500	DIL With Cooler							
507	Solder, SnPb	1.6	0.108	0.17	1.73	17.28	172.80	1728.00
502	TE Cooler	1.8	43.717	78.69	786.91	7082.15	62952.48	550834.20
505	Insulating Tube	1.8	0.68	1.22	12.24	110.16	979.20	7344.00
501	DIL Package	1.8	23.18	41.72	417.24	3755.16	33379.20	250344.00
600	Fiber Assembly							
601	Heat Shrink,.027"	2	0.0031	0.01	0.06	0.62	6.20	62.00
601	Solder Ball, AuSn	2	0.23377	0.47	4.68	46.75	467.54	4675.40
601	Fiber, 9μm, Lens	2	54.58331	109.17	1091.67	9825.00	87333.30	654999.72
601	Tube, Plated	2	2.67567	5.35	53.51	535.13	5351.34	53513.40
700	Untested SLD							
706	Gold wire,.002"	1.6	0.0166	0.03	0.27	2.66	26.56	265.60
703	Epoxy, H70E	1.6	0.00032	0.00	0.01	0.05	0.51	5.12
728	Heat Shrink,.125"	1.25	0.02475	0.03	0.31	3.09	30.94	309.38
726	Black Ink	1.25	0.07849	0.10	0.98	9.81	98.11	981.13
707	Preform, InSn	1.6	3.13745	5.02	50.20	501.99	5019.92	50199.20

APPENDIX XI (continued)

Material Costs Cost, $

Seq.	Description	Quantity	Each piece	1	10	100	1000	10000
727	Epoxy, Torrseal	1.25	0.00045	0.00	0.01	0.06	0.56	5.63
723	Cleaned Cover	1.3	1.26571	1.65	16.45	164.54	1645.42	16454.23
710	Sleeve Clamp	1.4	5.5575	7.78	77.81	700.25	6224.40	46683.00
711	Solder, InSn	1.4	0.21475	0.30	3.01	30.07	300.65	3006.50
701	Thermistor	1.6	8.42843	13.49	134.85	1213.69	10788.39	80912.93
710	Screws, 0-80	1.4	1.14192	1.60	15.99	159.87	1598.69	15986.88
710	Fiber Support	1.4	10.13571	14.19	141.90	1277.10	11352.00	99329.96
701	Ceramic, S/off	1.6	17.72114	28.35	283.54	2551.84	22683.06	170122.94
717	Detector Assy	1.3	15.60663	20.29	202.89	1825.98	16230.90	142020.33
800	Tested SLD							
808	Label, ESD	1	0.092	0.09	0.92	9.20	92.00	920
808	Label, Contents	1	0.12	0.12	1.20	12.00	120.00	1200
808	Label, Warning	1	0.19	0.19	1.90	19.00	190.00	1900
808	Label, Danger	1	0.19	0.19	1.90	19.00	190.00	1900
808	Label, DIL	1	0.137	0.14	1.37	13.70	137.00	1370
808	Foam, .5"	1	0.35	0.35	3.50	35.00	350.00	3500
808	Foam, .25"	1	0.6	0.60	6.00	60.00	600.00	6000
808	Box	1	1.05	1.05	10.50	105.00	1050.00	10500
	Total, $			5385.10	9511.63	46393.53	385614.72	3216069.11

Routing Costs Cost, $

Seq.	Description	Factor	Hrs/piece	1	10	100	1000	10000
100	Grown Wafer (1 in 10 good)							
101	Prepare Substrate		0.3036	39.89	39.89	39.89	119.68	1196.79
102	Grow Wafer		3.082	404.97	404.97	404.97	1214.92	12149.24
103	Inspect Wafer		0.1857	24.40	24.40	24.40	73.20	732.03
				0.00	0.00	0.00	0.00	0.00
200	Evaluated Wafer			0.00	0.00	0.00	0.00	0.00
201	Prepare Wafer		0.01	1.31	1.31	1.31	3.94	39.42
202	Deposit SiO2		0.1	13.14	13.14	13.14	39.42	394.20
203	Coat Photoresist		0.01	1.31	1.31	1.31	3.94	39.42
204	Align Mask		0.01	1.31	1.31	1.31	3.94	39.42
205	Develop Photoresist		0.6	78.84	78.84	78.84	236.52	2365.20
206	Open Contact		0.125	16.43	16.43	16.43	49.28	492.75
203A	Coat Photoresist		0.01	1.31	1.31	1.31	3.94	39.42
204A	Align Mask		0.01	1.31	1.31	1.31	3.94	39.42
205A	Develop Photoresist		0.6	78.84	78.84	78.84	236.52	2365.20
206A	Open Contact		0.125	16.43	16.43	16.43	49.28	492.75

APPENDIX XI (continued)

Routing Costs				Cost, $				
Seq.	Description	Factor	Hrs/piece	1	10	100	1000	10000
207	Clean, J100		0.05	6.57	6.57	6.57	19.71	197.10
208	Deposit AuZn		0.1	13.14	13.14	13.14	39.42	394.20
209	Strip AuZn		0.02	2.63	2.63	2.63	7.88	78.84
210	P Metal Evap.		0.4	52.56	52.56	52.56	157.68	1576.80
211	Mount Wafer		0.01	1.31	1.31	1.31	3.94	39.42
212	Clean J100		0.05	6.57	6.57	6.57	19.71	197.10
213	N Metal Evap.		0.4	52.56	52.56	52.56	157.68	1576.80
214	Fast Alloy		0.05	6.57	6.57	6.57	19.71	197.10
215	N Metal Evap.		0.2	26.28	26.28	26.28	78.84	788.40
216	Evaluation Cleave		0.2	26.28	26.28	26.28	78.84	788.40
217	Load Coater		0.2	26.28	26.28	26.28	78.84	788.40
218	Coat Facet		0.2	26.28	26.28	26.28	78.84	788.40
219	Reload Coater		0.125	16.43	16.43	16.43	49.28	492.75
220	Coat Facet		0.2	26.28	26.28	26.28	78.84	788.40
221	Unload Coater		0.1	13.14	13.14	13.14	39.42	394.20
222	Separate Scribe		0.5	65.70	65.70	65.70	197.10	1971.00
223	Visual Inspection		0.25	32.85	32.85	32.85	98.55	985.50
224	Manual Bond		0.5	65.70	65.70	65.70	197.10	1971.00
225	Clean Assy.		0.1	13.14	13.14	13.14	39.42	394.20
226	Inspect Assy.		0.1	13.14	13.14	13.14	39.42	394.20
227	Test Power		0.25	32.85	32.85	32.85	98.55	985.50
228	Test Vf		0.05	6.57	6.57	6.57	19.71	197.10
229	Test Wavelength		0.5	65.70	65.70	65.70	197.10	1971.00
230	Burn in		0.01	1.31	1.31	1.31	3.94	39.42
231	Test Power		0.25	32.85	32.85	32.85	98.55	985.50
232	Interpret Data		0.1	13.14	13.14	13.14	39.42	394.20
300	Coated Chips							
301	Cleave Bars	2.5	0.00062	0.02	0.20	2.04	20.37	203.67
302	Load Coater	2.5	0.00031	0.01	0.10	1.02	10.18	101.84
303	Coat Facet	2.5	0.00031	0.01	0.10	1.02	10.18	101.84
304	Reload Coater	2.5	0.00031	0.01	0.10	1.02	10.18	101.84
305	Coat Facet	2.5	0.00031	0.01	0.10	1.02	10.18	101.84
306	Unload Coater	2.5	0.00016	0.01	0.05	0.53	5.26	52.56
307	Scribe Chips	2.5	0.00156	0.05	0.51	5.12	51.25	512.46
308	Inspect Chips	2.5	0.00078	0.03	0.26	2.56	25.62	256.23
400	Assembled Submount							
401	Manual Bond	2	0.05	1.31	13.14	131.40	1314.00	13140.00
402	Clean Assy.	2	0.01	0.26	2.63	26.28	262.80	2628.00
403	Inspect Assy.	2	0.01	0.26	2.63	26.28	262.80	2628.00
404	Test Power	1.8	0.05	1.18	11.83	118.26	1182.60	11826.00

APPENDIX XI (continued)

Routing Costs				Cost, $				
Seq.	Description	Factor	Hrs/piece	1	10	100	1000	10000
405	Burn in	1.8	0.005	0.12	1.18	11.83	118.26	1182.60
406	Test Power	1.8	0.05	1.18	11.83	118.26	1182.60	11826.00
407	Inspect Assy.	1.6	0.017	0.36	3.57	35.74	357.41	3574.08
500	DIL with Cooler							
501	Clean Package	1.8	0.017	0.40	4.02	40.21	402.08	4020.84
502	Clean Coolers	1.8	0.034	0.80	8.04	80.42	804.17	8041.68
503	Solder Cooler	1.8	0.1	2.37	23.65	236.52	2365.20	23652.00
504	Clean Assy.	1.8	0.017	0.40	4.02	40.21	402.08	4020.84
505	Fit Tubes	1.8	0.017	0.40	4.02	40.21	402.08	4020.84
506	Test Cooler	1.8	0.017	0.40	4.02	40.21	402.08	4020.84
507	Solder Wires	1.6	0.017	0.36	3.57	35.74	357.41	3574.08
600	Fiber Assembly							
601	Solder Tube	2	0.043	1.13	11.30	113.00	1130.04	11300.40
602	Shrink Tubing	1.6	0.043	0.90	9.04	90.40	904.03	9040.32
603	Label Lot	1.6	0.006	0.13	1.26	12.61	126.14	1261.44
700	Untested SLD							
701	Solder Thermistor	1.6	0.034	0.71	7.15	71.48	714.82	7148.16
702	Clean Assy.	1.6	0.0085	0.18	1.79	17.87	178.70	1787.04
703	Epoxy Submount	1.6	0.0085	0.18	1.79	17.87	178.70	1787.04
704	Bake	1.6	0.0001	0.00	0.02	0.21	2.10	21.02
705	Remove Spacers	1.6	0.0085	0.18	1.79	17.87	178.70	1787.04
706	Wire Bond	1.6	0.01	0.21	2.10	21.02	210.24	2102.40
707	Solder Submount	1.6	0.05	1.05	10.51	105.12	1051.20	10512.00
708	Wire Bond	1.6	0.01	0.21	2.10	21.02	210.24	2102.40
709	Optimize Align.	1.6	0.067	1.41	14.09	140.86	1408.61	14086.08
710	Clamp Fiber	1.4	0.067	1.23	12.33	123.25	1232.53	12325.32
711	Solder Feedthroug	1.4	0.067	1.23	12.33	123.25	1232.53	12325.32
712	Recover Power	1.4	0.083	1.53	15.27	152.69	1526.87	15268.68
713	Bake	1.4	0.0001	0.00	0.02	0.18	1.84	18.40
714	Recover Power	1.4	0.083	1.53	15.27	152.69	1526.87	15268.68
715	Bake	1.4	0.0001	0.00	0.02	0.18	1.84	18.40
716	Test Power	1.4	0.083	1.53	15.27	152.69	1526.87	15268.68
717	Epoxy Photodiode	1.3	0.017	0.29	2.90	29.04	290.39	2903.94
718	Bake	1.3	0.0001	0.00	0.02	0.17	1.71	17.08
719	Wire Bond	1.3	0.01	0.17	1.71	17.08	170.82	1708.20
720	Test Photodiode	1.3	0.01	0.17	1.71	17.08	170.82	1708.20
721	Fine Leak Test	1.3	0.0417	0.71	7.12	71.23	712.32	7123.19
722	Inspect	1.3	0.018	0.31	3.07	30.75	307.48	3074.76
723	Seam Seal	1.3	0.01	0.17	1.71	17.08	170.82	1708.20

APPENDIX XI (continued)

Routing Costs				Cost, $				
Seq.	Description	Factor	Hrs/piece	1	10	100	1000	10000
724	Fine Leak Test	1.3	0.0417	0.71	7.12	71.23	712.32	7123.19
725	Gross Leak Test	1.27	0.017	0.28	2.84	28.37	283.69	2836.93
726	Mark Devices	1.25	0.034	0.56	5.58	55.85	558.45	5584.50
727	Apply Sealant	1.25	0.0085	0.14	1.40	13.96	139.61	1396.13
728	Add Heatshrink	1.25	0.0085	0.14	1.40	13.96	139.61	1396.13
800	Tested SLD							
801	Test Power	1.25	0.091	1.49	14.95	149.47	1494.68	14946.75
802	Thermal Shock	1.2	0.001	0.02	0.16	1.58	15.77	157.68
803	Burn in	1.2	0.01	0.16	1.58	15.77	157.68	1576.80
804	Test power	1.2	0.091	1.43	14.35	143.49	1434.89	14348.88
805	Test power, Hot	1.15	0.091	1.38	13.75	137.51	1375.10	13751.01
806	Test Wavelength	1.1	0.091	1.32	13.15	131.53	1315.31	13153.14
807	Inspection	1	0.0078	0.10	1.02	10.25	102.49	1024.92
808	Pack Devices	1	0.034	0.45	4.47	44.68	446.76	4467.60
	Total,$			1361.64	1688.36	4955.58	40278.43	402784.30

Summary	Cost, $				
Quantity / annum	1	10	100	1000	10000
Material Cost	5385.10	9511.63	46393.53	385614.72	3216069.11
Handling Cost	605.82	1070.06	5219.27	43381.66	361807.77
Direct Labor Cost	1361.64	1688.36	4955.58	40278.43	402784.30
Fixed Overhead	5473.80	6787.22	19921.43	161919.29	1619192.87
Cost of Sales	12826.37	19057.28	76489.81	631194.09	5599854.05
Unit Cost	12826.37	1905.73	764.90	631.19	559.99